LARGE SCALE DYNAMICS OF PRECIPITATION FRONTS IN THE TROPICAL ATMOSPHERE: A NOVEL RELAXATION LIMIT [*]

DARGAN M. W. FRIERSON [†], ANDREW J. MAJDA [‡], AND OLIVIER M. PAULUIS [§]

Abstract. A simplified set of equations is derived systematically below for the interaction of large scale flow fields and precipitation in the tropical atmosphere. These equations, the Tropical Climate Model, have the form of a shallow water equation and an equation for moisture coupled through a strongly nonlinear source term. This source term, the precipitation, is of relaxation type in one region of state space for the temperature and moisture, and vanishes identically elsewhere in the state space of these variables. In addition, the equations are coupled nonlinearly to the equations for barotropic incompressible flow. Several mathematical features of this system are developed below including energy principles for solutions and their first derivatives independent of relaxation time. With these estimates, the formal infinitely fast relaxation limit converges to a novel hyperbolic free boundary problem for the motion of precipitation fronts from a large scale dynamical perspective. Elementary exact solutions of the limiting dynamics involving precipitation fronts are developed below and include three families of waves: fast drying fronts as well as slow and fast moistening fronts. The last two families of waves violate Lax's Shock Inequalities; nevertheless, numerical experiments presented below confirm their robust realizability with realistic finite relaxation times. From the viewpoint of tropical atmospheric dynamics, the theory developed here provides a new perspective on the fashion in which the prominent large scale regions of moisture in the tropics associated with deep convection can move and interact with large scale dynamics in the quasi-equilibrium approximation.

Key words. tropical atmospheric dynamics, equatorial waves, tropical convection, moisture, hyperbolic PDE, nonlinear relaxation equations, hyperbolic free boundary problems

MSC 2000 subject classifications: 86A10 Meteorology and atmospheric physics 35L67 PDE of hyperbolic type, Shocks and singularities

1. Introduction

One of the striking observational discoveries over the last few decades is the profound impact of the interaction of water vapor and planetary scale dynamics in the tropics on monthly, seasonal, and even decadal prediction of weather and climate in the midlatitudes [21]. Contemporary comprehensive computer models (known as general circulation models or GCM's) are currently incapable of adequately resolving or parameterizing these interactions on time scales appropriate for seasonal prediction as well as climate change projections [38]. Given the complexity of contemporary GCM's, one important theoretical thrust in the atmospheric science community is the development of simplified models for the parameterization of the interaction of moisture and large scale dynamics which retain fidelity with crucial features of the observational record ([9], [32], [33], [42], [11], [43], [28], [27], [26]). Observations show that moisture-coupled large scale waves in the atmosphere often move at speeds that are much slower than the dry gravity wave speed ([21], [40]); the theoretical prediction of these slower wave speeds through the reduction of stability of the atmosphere from deep moist convection is one important result of the previously mentioned theoretical

[†]Program in Applied and Computational Mathematics, Princeton University, Fine Hall, Washington Rd., Princeton, NJ 08544 (frierson@math.princeton.edu).

[‡]Department of Mathematics and Center for Atmosphere Ocean Science, Courant Institute of Mathematical Sciences, New York University, 251 Mercer St., New York, NY 10012 (jonjon@cims.nyu.edu).

[§]Center for Atmosphere Ocean Science, Courant Institute of Mathematical Sciences, New York University, 251 Mercer St., New York, NY 10012 (pauluis@cims.nyu.edu).

work. [34] have developed a simplified Quasi-Equilibrium Tropical Circulation Model (QTCM) based on this principle of reduced stability in moist regions.

The main thrust of this paper is to develop a new mathematical theory for the propagation and interaction of precipitation fronts from a large scale dynamical perspective motivated by the work mentioned above. In section 2, we present a detailed derivation, starting from the Boussinesq equations and the equations for bulk cloud microphysics, of a family of simplified prototype tropical climate models for the interaction of moisture with large scale dynamics. In spirit these models have similar features to the QTCM of [34] but a detailed systematic self-contained derivation is merited as an introduction to these topics for the applied mathematics community. These simplified equations, the Tropical Climate Model, have the form of a shallow water equation and a scalar equation for moisture coupled through a strongly nonlinear source term. This term, the precipitation, is of relaxation type in one region of state space for the temperature and moisture while the nonlinearities vanish identically elsewhere in the state space. In addition, these equations are coupled nonlinearly to the equations for barotropic incompressible flow in two horizontal space dimensions. The reader mostly interested in PDE aspects can skip directly to section 3 without reading section 2. In section 3, several mathematical features of this system are developed including energy principles for solutions and their first derivatives independent of relaxation time. The estimates established in section 3 allow us to discuss the formal infinitely fast relaxation limit in section 4, which is a novel hyperbolic free boundary problem for the motion of precipitation fronts from a large scale dynamical perspective. Such precipitation fronts are in the Sobolev space H^1, but have jumps in their first derivatives. Elementary exact solutions of the limiting dynamics involving precipitation fronts are developed in detail in section 4 and include three families of waves with discontinuities in the first derivatives: fast drying fronts as well as slow and fast moistening fronts. The last two families of moistening waves violate Lax's shock inequalities for moving discontinuities in hyperbolic systems [23]. Nevertheless, section 5 contains detailed numerical experiments which confirm the robust realizability of all three families of precipitation fronts with realistic finite relaxation times.

From the viewpoint of applied mathematics, this paper studies a new class of strongly nonlinear relaxation systems which has completely novel phenomena as well as features in common with the established applied mathematical theories of relaxation limits for conservation laws ([7], [17], [18]) and waves in reacting gas flows ([22]; [8], [4]). Some of the similarities and differences with the phenomena for reacting gas flow are discussed briefly at the end of section 5 while the general energy decay principle established in section 3 is a common feature with relaxation limits [7]. Section 6 of the paper establishes briefly that similar effects also occur in elementary steady state models of the tropical circulation with both forcing and damping. The paper concludes with a list of accessible open problems in applied analysis motivated by the present work. The reader interested in further disciplinary application in atmospheric science of the theory developed here can consult the forthcoming paper of the authors [35]. A high resolution balanced numerical scheme for the idealized Tropical Climate Model in section 2 has been developed very recently [19]; that paper contains a systematic study of the multi-dimensional geophysical effects of the complete coupled Tropical Climate Model on the elementary exact solutions from section 4 of this paper.

2. Simplified Model Dynamics

2.1. The Hydrostatic Boussinesq Equations on the Equatorial β-plane.
We begin with the constant buoyancy frequency version of the hydrostatic Boussinesq equations on the equatorial β-plane as the dynamical core, since we are interested in lower and middle troposphere dynamics. The Boussinesq equations are obtained by expanding the Navier-Stokes equations in a power series about a background state which is a function of height. This filters the fast and meteorologically insignificant sound waves from the system. The hydrostatic approximation of the vertical momentum equation, which is justified by the small aspect ratio of the flow, is additionally employed. The equatorial β-plane approximation is a linearization of the Coriolis parameter about the equator (where it is zero). See texts such as [13], [36], and [24] for derivations and further discussion of these models.

The hydrostatic Boussinesq equations on a β-plane are as follows:

$$\frac{D\mathbf{U}}{Dt} = -\beta y \mathbf{U}^{\perp} - \nabla p + S_{\mathbf{U}} \tag{2.1}$$

$$\nabla \cdot \mathbf{U} + \frac{\partial w}{\partial z} = 0 \tag{2.2}$$

$$\frac{DT}{Dt} = -\frac{T_0 N^2}{g} w + S_T \tag{2.3}$$

$$\frac{\partial p}{\partial z} = \frac{gT}{T_0} \tag{2.4}$$

where

$$\frac{D}{Dt} = \frac{\partial}{\partial t} + \mathbf{U} \cdot \nabla + w \frac{\partial}{\partial z} \tag{2.5}$$

is the advective derivative, and (x,y,z) are the eastward, northward, and upward (above sea level) distances, t is time, $U=(u,v)$ is the zonal (eastward) and meridional (northward) velocities, w is the vertical velocity, and T is the perturbation temperature. The full temperature in this system (including the background state) is $T_0 + \frac{\partial \bar{T}}{\partial z} z + T$. The vertical gradient of the temperature determines its dry stability to vertical perturbations, and its buoyancy frequency. The buoyancy frequency of the background state is $N = \left(\frac{g}{T_0} \left(\frac{\partial \bar{T}}{\partial z} + \frac{g}{c_p} \right) \right)^{\frac{1}{2}}$, assumed here to be constant, as is the mean basic state temperature, T_0.

The pressure, p, is always a reduced pressure divided by a constant density factor which is omitted; thus the units for this reduced pressure are given by

$$[p] = \frac{L^2}{T^2} \tag{2.6}$$

where $[f] =$ units of f. We utilize the following standard values for parameters: $T_0 = 300\ K$, the mean atmospheric temperature in Kelvin; $N = 10^{-2}\ s^{-1}$, the buoyancy frequency; $g = 9.8\ m/s^2$, gravitational acceleration; $c = 50\ m/s$, the wave speed; $H_T = 15.75\ km$, the tropopause height, obtained from the relation $H_T = \frac{c\pi}{N}$; and $\beta = 2.28 \times 10^{-11}\ m^{-1} s^{-1}$.

We now nondimensionalize these equations, using the following units: $L_E = \sqrt{\frac{c}{\beta}} \approx 1500\ km$, the typical equatorial length scale; $T_E = \frac{L_E}{c} \approx 8.3\ hrs$, the equatorial

timescale; $\bar{\alpha} = \frac{H_T N^2 T_0}{\pi g} \approx 15 \ K$, the typical temperature scale; and $P = c^2$, the pressure scale. Further derived units include the vertical velocity scale $W = \frac{H_T}{\pi T_E} \approx .18 \ m/s$.

Using the above units and parameters, we have the nondimensional hydrostatic Boussinesq equations on a β-plane:

$$\frac{D\hat{\mathbf{U}}}{D\hat{t}} = -\hat{y}\hat{\mathbf{U}}^\perp - \hat{\nabla}\hat{p} + \hat{S}_{\mathbf{U}} \qquad (2.7)$$

$$\hat{\nabla}\cdot\hat{\mathbf{U}} + \frac{\partial\hat{w}}{\partial\hat{z}} = 0 \qquad (2.8)$$

$$\frac{D\hat{T}}{D\hat{t}} = -\hat{w} + \hat{S}_T \qquad (2.9)$$

$$\frac{\partial\hat{p}}{\partial\hat{z}} = \hat{T} \qquad (2.10)$$

where the hats represent nondimensional variables scaled by the units described above. From this point on, we drop the hats and consider all variables to be nondimensional quantities. The boundary conditions assumed here are no normal flow at the top and bottom of the troposphere, i.e., $w = 0$ at $z = 0, \pi$.

2.2. Vertical Decomposition and Galerkin Expansion. The flow in the tropics is primarily in the first baroclinic mode, that is, with winds in the lower troposphere of opposite sign and equal magnitude to those in the upper troposphere. First baroclinic mode models have been used in many studies of tropical atmospheric dynamics dating back to [31] and [12]. In these models, there is one temperature, representing a typical midtropospheric temperature, and the first baroclinic mode velocity. We derive this model more rigorously from the hydrostatic Boussinesq equations by performing a Galerkin truncation, keeping two velocity modes. We retain the barotropic mode as well as the baroclinic mode, unlike the above studies. Keeping the barotropic mode is necessary for the study of tropical-extratropical interactions, where transport of momentum from the barotropic and baroclinic mode is an important effect [25].

We begin by performing a vertical decomposition of the variables as such:

$$\mathbf{U} = \bar{\mathbf{U}} + \mathbf{U}' \qquad (2.11)$$

$$p = \bar{p} + p' \qquad (2.12)$$

and so on, where $\bar{\mathbf{U}} = \langle\mathbf{U}, 1\rangle$, $\bar{p} = \langle p, 1\rangle$ are the depth-independent barotropic modes (i.e., the orthogonal projection on 1), and $\langle f, g\rangle = \frac{1}{\pi}\int_0^\pi fg\,dz$. The quantities $\mathbf{U}', p'$ are baroclinic modes, with $\langle\mathbf{U}', 1\rangle = \langle p', 1\rangle = 0$.

The complete Galerkin expansion of baroclinic modes in nondimensional form is

$$p' = \Sigma_{j=1}^\infty p_j e_j(z) \qquad (2.13)$$

$$\mathbf{U}' = \Sigma_{j=1}^\infty \mathbf{U}_j e_j(z) \qquad (2.14)$$

$$e_j(z) = \sqrt{2}cos(zj), 0 < z < \pi, j = 1, 2, ... \qquad (2.15)$$

(see Chapter 9 of [24]).

The projected free tropospheric nonlinear dynamics, obtained by substituting (2.11) and (2.12) into equations (2.7)-(2.10), are as follows: first, the barotropic mode

dynamics,

$$\frac{\bar{D}\bar{\mathbf{U}}}{Dt} + \langle \mathbf{U}' \cdot \nabla \mathbf{U}', 1 \rangle + \langle w' \frac{\partial \mathbf{U}'}{\partial z}, 1 \rangle + y\bar{\mathbf{U}}^{\perp} = -\nabla \bar{p} + \bar{S}_{\mathbf{U}} \tag{2.16}$$

$$\nabla \cdot \bar{\mathbf{U}} = 0 \tag{2.17}$$

where

$$\frac{\bar{D}}{Dt} = \frac{\partial}{\partial t} + \bar{\mathbf{U}} \cdot \nabla. \tag{2.18}$$

The vertical mean vertical velocity satisfies $\bar{w} = 0$. The baroclinic dynamics satisfy

$$\frac{\bar{D}\mathbf{U}'}{Dt} + \mathbf{U}' \cdot \nabla \bar{\mathbf{U}} + \mathbf{U}' \cdot \nabla \mathbf{U}' - \langle \mathbf{U}' \cdot \nabla \mathbf{U}', 1 \rangle$$

$$+ w' \frac{\partial \mathbf{U}'}{\partial z} - \langle w' \frac{\partial \mathbf{U}'}{\partial z}, 1 \rangle + y\mathbf{U}'^{\perp} = -\nabla p' + S'_{\mathbf{U}} \tag{2.19}$$

$$\frac{\bar{D}}{Dt}\left(\frac{\partial p'}{\partial z}\right) + \mathbf{U}' \cdot \nabla \left(\frac{\partial p'}{\partial z}\right) + w' \frac{\partial}{\partial z}\left(\frac{\partial p'}{\partial z}\right) = -w' + S_T. \tag{2.20}$$

In equation (2.20), we have used the relation $T = \frac{\partial p'}{\partial z}$ obtained from the hydrostatic equation; therefore equation (2.20) is the full buoyancy equation, not the barotropic or baroclinic parts as the velocity equations (2.16) and (2.19).

We create a simplified model for the dynamics of the free troposphere via Galerkin truncation of the baroclinic mode equations to the first baroclinic mode, as motivated above. It is important to point out that the first baroclinic approximation is strongly justified in areas of deep convection, where latent heating in the midtroposphere creates the baroclinic structure. However, in dry regions, this approximation begins to break down, due to vertical propagation of gravity waves which upset the vertical structure. Therefore some degree of care must be taken when interpreting results which rely strongly on behavior in dry regions.

Our assumptions about the baroclinic modes are as follows (all valid for $0 \leq z \leq \pi$):

$$p' = p_1 \sqrt{2} cos(z) \tag{2.21}$$

$$\mathbf{U}' = \mathbf{U}_1 \sqrt{2} cos(z) \tag{2.22}$$

$$T = p'_z = -p_1 \sqrt{2} sin(z) \tag{2.23}$$

$$w' = -\nabla \cdot \mathbf{U_1} \sqrt{2} sin(z). \tag{2.24}$$

First, this implies that the baroclinic interaction terms in the barotropic velocity equation (2.16) project directly; i.e., this equation becomes

$$\frac{\bar{D}\bar{\mathbf{U}}}{Dt} + \mathbf{U_1} \cdot \nabla \mathbf{U_1} + (\nabla \cdot \mathbf{U_1})\mathbf{U_1} + y\bar{\mathbf{U}}^{\perp} = -\nabla \bar{p} + \bar{S}_{\mathbf{U}}. \tag{2.25}$$

To derive the reduced dynamics for the baroclinic velocity field $\mathbf{U_1}$, we take the inner product of equation (2.19) above with $\sqrt{2}cos(z)$ under the ansatz above, giving the Galerkin projected baroclinic momentum equation

$$\frac{\bar{D}\mathbf{U_1}}{Dt} + \mathbf{U_1} \cdot \nabla \bar{\mathbf{U}} + y\mathbf{U_1}^{\perp} = -\nabla p_1 + S'_{\mathbf{U}}. \tag{2.26}$$

To derive the projected baroclinic buoyancy equation, we take the inner product of equation (2.20) above with $\sqrt{2}sin(z)$ and this yields the Galerkin truncated buoyancy equation,

$$\frac{\bar{D}p_1}{Dt} + \nabla \cdot \mathbf{U_1} = -S_T. \tag{2.27}$$

Through a mild abuse of notation, we still denote $S_T = \langle S_T, sin(z)\rangle$. This equation is often written in terms of T, with the identification from (2.23),

$$T = -p_1. \tag{2.28}$$

(Since this is the only temperature in the system, we denote the above by T rather than T_1 to be consistent with standard notation.) Maxima of T imply minima in pressure in the lower troposphere and maxima in the upper troposphere.

2.3. Physical Parameterizations. We now must consider the source terms $S_\mathbf{U}$ and S_T. The effects we want to capture are momentum damping by frictional drag, and three temperature source terms: the radiative cooling $S_{T,R}$, the sensible heat flux $S_{T,SH}$, and the precipitation $S_{T,P}$.

2.3.1. Momentum Damping, Radiative Cooling, and Sensible Heat Flux. We parameterize frictional dissipation in the atmosphere by relaxation of velocities to zero:

$$S_\mathbf{U} = -\bar{d}\mathbf{U}. \tag{2.29}$$

For surface velocities, one would expect relatively strong damping (for instance on the order of 5 day damping time), but for the upper troposphere, there is very little momentum drag. The momentum drag parameter $\bar{d}$ is therefore somewhat arbitrary for first baroclinic mode models. Studies such as [12] and [16] have been successful using values around $\bar{d} = (3.8 - 10\ days)^{-1}$. Here we utilize values similar to these, or consider the inviscid problem with $\bar{d} = 0$.

The standard parameterization for radiation in models of our complexity is Newtonian cooling, i.e., relaxation to a specified radiative equilibrium profile over a certain damping time. That is,

$$S_{T,R} = -d_T(T - T_{eq}) \tag{2.30}$$

where $d_T \approx (20\ days)^{-1}$. Since radiation acts as a net cooling within the atmosphere, we specify $T_{eq} < 0$.

We parameterize the sensible heat flux in a manner similar to the momentum damping, using a drag law formulation that relaxes temperatures to the surface value:

$$S_{T,SH} = d_{SH}(T_s - T) \tag{2.31}$$

where T_s is the sea surface temperature. The drag coefficient is typically selected to be $d_{SH} \approx (10\ days)^{-1}$.

Sensible heat fluxes in the tropical atmosphere are small compared to evaporative fluxes, radiative cooling, and precipitation. The ratio of evaporation to sensible heating is given by the Bowen ratio, which is typically on the order of .2 in the tropics [15]. We therefore often neglect sensible heating for simplicity in this model.

2.3.2. Precipitation.   The final diabatic term needed in the buoyancy equation is the precipitation, $S_{T,P}$. The parameterization of precipitation has been somewhat difficult historically in models of this complexity. Many studies (e.g., [13], [37]) have simply specified precipitation distributions, or constructed simple parameterizations based on sea surface temperature distributions, and then calculated the atmospheric response to this heating. However moisture not only drives the large scale flow, it is advected by the large scale flow as well. Therefore, for our parameterization of precipitation, we employ an active moisture equation so we can allow the flow to affect the precipitation distribution, and vice-versa. Other studies which use active moisture budgets to determine the precipitation within first baroclinic mode models include [32], [33], [34], and [6].

In the tropics, most of the moisture is concentrated in the lower troposphere. For our simplified dynamics, we will derive an equation for q_v, the mixing ratio of water vapor in the atmosphere, which is vertically averaged as in [34]. The motivation for the closure approach is best understood by looking at the equations for bulk cloud microphysics which illustrate the full moisture dynamics. Ultimately we will get a simplified equation for $q(x,y,t) = \langle q_v, 1 \rangle$.

Bulk Cloud Microphysics

To examine the conservation laws present in the microphysical system, we consider the set of equations without radiative effects or sensible heat fluxes. We derive conservation laws for the moist static energy, an energy which accounts for the moisture content of the air (which releases latent heat when it condenses), and the total moisture content of the air. The fully dimensional bulk microphysical equations are the following:

$$c_p \frac{DT}{Dt} = -\frac{c_p T_0 N^2}{g} w + L(C_d - E_r) \tag{2.32}$$

$$\frac{Dq_v}{Dt} = -C_d + E_r \tag{2.33}$$

$$\frac{Dq_c}{Dt} = C_d - A_r - C_r \tag{2.34}$$

$$\frac{Dq_r}{Dt} = \frac{\partial(v_t q_r)}{\partial z} + A_r + C_r - E_r \tag{2.35}$$

where q_v is the mixing ratio (mass of constituent divided by mass of dry air) of water vapor, q_c is the mixing ratio of cloud water, and q_r is the mixing ratio of rain. Of the various conversion terms, C_d is the condensation of water vapor, E_r is the reevaporation of rain into unsaturated air, A_r is the autoconversion of cloud water into rain, and C_r is the rain collection (falling rain gathering cloud water into rain). v_t is the terminal (downward) velocity of rain droplets. Cloud resolving numerical models and some general circulation models have parameterizations of each of these processes, and often utilize distributions of droplet size, of which the conversion processes and fall speed are a function. See [10] for further discussion of these parameterizations.

An important relation for the parameterization of the condensation and evaporation is the Clausius-Clapeyron equation, a first order differential equation for the saturation vapor pressure e_s as a function of temperature. The Clausius-Clapeyron equation is:

$$\frac{de_s}{dT} = \frac{Le_s}{R_v T^2} \tag{2.36}$$

and the saturation specific humidity satisfies $q_{v,s} = \frac{R_d e_s}{R_v p}$, where R_d and R_v are the gas constants for dry air and water vapor, respectively, and p is the pressure. Condensation occurs when the specific humidity exceeds its saturation value, i.e., when $q_v > q_{v,s}$. Specifically,

$$q_v < q_{v,s}, q_c = 0, C_d = 0 \tag{2.37}$$

$$q_v > q_{v,s}, q_c \geq 0, C_d = \infty. \tag{2.38}$$

The latter implies that $q_c \geq 0 \Leftrightarrow q_v = q_{v,s}$. [29] discuss various subtle issues for these parameterizations in the context of turbulent mixing problems.

Conservation Principles for Bulk Cloud Microphysics

There are two key quantities in this microphysics model with conservation laws. Firstly, the moist static energy, $m = c_p T + \frac{c_p T_0 N^2}{g} z + L q_v$ is conserved, as can be seen from adding (2.32) and (2.33) and using $w = \frac{Dz}{Dt}$:

$$\frac{Dm}{Dt} = 0. \tag{2.39}$$

The moist static energy, which can be rewritten in the familiar form $m = c_p(T + \frac{\partial \bar{T}}{\partial z} z) + gz + L q_v$, includes the thermal energy, the gravitational energy, and a moisture component reflecting the thermal energy increase that would occur if condensation occurs.

Further, by adding equations (2.33), (2.34), (2.35), we see that the total moisture $Q = q_v + q_c + q_r$ is conserved except for precipitation:

$$\frac{DQ}{Dt} = \frac{\partial(v_t q_r)}{\partial z} \tag{2.40}$$

where the right hand side is the divergence of the rain water flux, falling at its terminal velocity. The precipitation is defined as the flux of this term evaluated at the ground, i.e., $P = v_t q_r|_{z=0}$. Clearly P satisfies the constraint $P \geq 0$. The equations in (2.34) and (2.35) imply that the total liquid water $q_l = q_c + q_r$ satisfies

$$\frac{Dq_l}{Dt} = C_d - E_R + \frac{\partial v_t q_r}{\partial z}. \tag{2.41}$$

Keeping these conservation laws for the full system in mind, we now proceed with vertical averaging of the equations, and make several approximations appropriate to the level of complexity of the model. Our goal will be one equation for the vertically integrated water vapor, and parameterizations for the latent heating and evaporation.

2.3.3. Vertical Averaging of the Moisture Equation. After vertical averaging of the equations in (2.39) and (2.40) (i.e., taking the inner product of these quantities with 1), we have the following conservation equations, for liquid water

$$\langle \frac{Dq_l}{Dt}, 1 \rangle = \langle C_d - E_r, 1 \rangle - P \tag{2.42}$$

and moist static energy

$$\langle \frac{Dm}{Dt}, 1 \rangle = 0 \tag{2.43}$$

while the conservation of vertically integrated water vapor (equation (2.33)) becomes

$$\langle \frac{Dq_v}{Dt}, 1 \rangle = -\langle C_d - E_r, 1 \rangle. \tag{2.44}$$

We now discuss additional approximations to these vertically averaged moisture equations.

Moisture Equation Approximation 1

We first assume a quasi-steady state from faster dynamics for vertically integrated liquid water q_l, i.e.,

$$\langle \frac{Dq_l}{Dt}, 1 \rangle = 0. \tag{2.45}$$

This is justified by the faster microphysical timescales which determine the rate of change of liquid water.

Therefore, from equation (2.42), we have

$$P = \langle C_d - E_r, 1 \rangle. \tag{2.46}$$

Substituting the above into equation (2.44) then implies that

$$\langle \frac{Dq_v}{Dt}, 1 \rangle = -P. \tag{2.47}$$

This approximation has allowed us to eliminate the liquid water variables as prognostic variables, and consider the water vapor variable alone.

Next, we make approximations regarding the vertical structure of water vapor to simplify our budgets further. We first separate the water vapor into vertical average and mean zero components as above:

$$q_v = \bar{q}_v + q_v'. \tag{2.48}$$

Rearranging the terms in the advective derivative, the equation for the mean tendency of water vapor is therefore

$$\langle \frac{Dq_v}{Dt}, 1 \rangle = \frac{\bar{D}\bar{q}_v}{Dt} + \langle \mathbf{U}' \cdot \nabla q_v', 1 \rangle$$
$$+ \langle w' \frac{\partial q_v'}{\partial z}, 1 \rangle - (w' q_v')|_{z=0} = -P. \tag{2.49}$$

The surface turbulent flux term $(w' q_v')|_{z=0}$ is the evaporation flux E, i.e.,

$$(w' q_v')|_{z=0} = E. \tag{2.50}$$

Moisture Equation Approximation 2

We assume that there is a background mean moisture gradient (as for the temperature in the Boussinesq equations) that is obtained from a mean sounding. We assume that this background moisture gradient is the dominant contribution to the vertical motion, that is,

$$\langle w' \frac{\partial q_v'}{\partial z}, 1 \rangle = \bar{Q} \nabla \cdot \mathbf{U_1}. \tag{2.51}$$

The key approximation is that the "gross moisture stratification" $\bar{Q}$ is independent of the integrated moisture content.

Note that $\bar{Q}$ satisfies $\bar{Q} > 0$ since typical moisture soundings fall off approximately exponentially with scale heights of a few kilometers. The parameter $\bar{Q}$ is quite important for the dynamics; it reduces the stability in moist regions, as described in the introduction. We will return to this parameter later.

Moisture Equation Approximation 3

For simplicity, we ignore turbulent fluctuations and assume

$$\langle \mathbf{U}' \cdot \nabla q_v', 1 \rangle = 0, \tag{2.52}$$

that is, perturbation moisture is only advected by the mean flow. This approximation could be refined if needed for other modeling studies.

Simplified Dynamics for Moisture Equation

Using equations (2.50), (2.51), and (2.52) in equation (2.49), we have, with $q \equiv \langle q_v, 1 \rangle$, the simplified dynamics for moisture:

$$\frac{\bar{D}q}{Dt} + \bar{Q} \nabla \cdot \mathbf{U_1} = E - P \tag{2.53}$$

where $\bar{Q}$ is the prescribed gross moisture stratification. We now discuss the evaporation and precipitation parameterizations.

Evaporation Parameterization

The evaporation is parameterized by a drag law formulation, that is,

$$E = d_q(q_s(T_s) - q). \tag{2.54}$$

A typical value of the inverse evaporative timescale is $d_q \approx (10 days)^{-1}$. The temperature T_s used to calculate the saturation mixing ratio at the surface is the sea surface temperature, which we specify as a function of x and y in this model.

2.3.4. Precipitation Parameterization.   Our spatial units for the dynamics is 1500 km, so the tacit assumption operating is that we are considering effects of moisture on large spatial scales. On such large scales, it is natural to model the precipitation based on the formulation of Betts and Miller ([2]; [3]) who relax temperature and humidity back to a reference profile when some convective criterion is met. Within our model, when there is enough moisture for convection, we relax the humidity back to a significant fraction of the saturation value, $\tilde{q}$. More precisely,

$$P = \frac{1}{\tau_c}(q - \tilde{q}(T))^+ \tag{2.55}$$

where $\tilde{q}$ is a prescribed function of the atmospheric temperature (possibly a nonlinear function), and τ_c is a convective adjustment time. [34] and [3] use relaxation times of the order $\tau_c \approx 2hrs$, whereas [5] estimate $\tau_c \approx 12hrs$ from current observations.

Two types of functions are typically used for the moisture saturation parameterization. The first of these is a precipitation threshold, independent of T, i.e.,

$$\tilde{q}(T) = \hat{q}. \tag{2.56}$$

This parameterization is the simplest mathematically, and is physically justified since atmospheric temperatures are approximately uniform across the tropics. There is also

observational data which correlates the precipitation in the tropics with the humidity content [39].

A second parameterization, utilized by [34], is proportional to temperature:

$$\tilde{q}(T) = T. \tag{2.57}$$

This is known as the CAPE parameterization, since it is based on the quasi-equilibrium of convectively available potential energy (CAPE), which is the integrated buoyancy a surface parcel of air can obtain [10]. CAPE increases with the surface humidity since more latent heat is released for parcels that are more humid, which are therefore more buoyant relative to the environment. CAPE also decreases with the temperature of the environment, since it is easier to be buoyant in colder air. The proper expression for CAPE in the nondimensional units explained above for our system is $q - T$, so CAPE is kept in quasi-equilibrium by using the saturation criterion (2.57). Full general circulation model convection schemes such as Arakawa-Schubert [1] and [3] would reduce to this in the first baroclinic mode system. Thus, the parameterizations in (2.56) or (2.57) together with (2.55) are simple prototype models for the behavior of GCM's.

In this paper, we build a class of convective parameterizations which contain both of these options by performing our analysis on the parameterization

$$\tilde{q}(T) = \hat{q} + \alpha T \tag{2.58}$$

with $0 \leq \alpha \leq 1$ and $\hat{q} > 0$. Actually, all the analysis developed below only requires $-\bar{Q} < \alpha < +\infty$. The use of various parameterizations for precipitation permits us to study the variability of dynamics with different convective parameterizations, an important practical topic.

For the arguments in section 3 where we differentiate the equations, it is convenient to keep in mind a smooth regularized version of (2.55), where

$$P = \frac{1}{\tau_c} \phi(q - \tilde{q}(T)) \tag{2.59}$$

with $\phi(s)$ a monotone smooth approximation to $(s)^+$ and satisfying

$$\phi(s) \geq 0$$
$$\phi(s) \equiv 1 \text{ for } s > 0$$
$$\phi(s) \equiv 0 \text{ for } s < 0$$
$$\phi'(s) \geq 0. \tag{2.60}$$

Since $\hat{q} \geq 0$, with (2.60) we also automatically have

$$(s + \hat{q})\phi(s) \geq 0. \tag{2.61}$$

which is obviously satisfied for (2.55). In the zero relaxation limit, one can recover (2.55) through letting $\phi(s)$ depend on τ_c and converge to $(s)^+$ as $\tau_c \to 0$ in standard fashion. Without further comment, we assume that P is smooth with the above structure when we differentiate the equations in section 3 below.

Nondimensional Moisture Equation

We nondimensionalize moisture by the scale of temperature variations divided by the latent heat coefficient L: $Q = \frac{\bar{\alpha}}{L}$, where $\bar{\alpha} = \frac{H_T N^2 T_0}{\pi g}$ is the temperature scale from section 2.1.

Our final nondimensional moisture equation is then the following:

$$\frac{\bar{D}q}{Dt} + \bar{Q}\nabla \cdot \mathbf{U_1} = d_q(q_s(T_s) - q) - P. \tag{2.62}$$

All of the parameters, $\bar{Q}$, $\hat{q}$, etc. have now taken nondimensional values.

This equation and the precipitation parameterization are used in the temperature equation with the following approximation.

2.3.5. Vertical Heating: Approximation 4.   Consistent with the above approximations we assume that all vertical heating (convective, radiative, and sensible) goes into the first baroclinic mode, so that the fully dimensional temperature equation becomes:

$$\frac{DT}{Dt} + w = LP\sqrt{2}sin(\frac{z}{H}) - d_T(T - T_{eq})\sqrt{2}sin(\frac{z}{H})$$
$$+ d_{SH}(T_s - T)\sqrt{2}sin(\frac{z}{H}). \tag{2.63}$$

Note that equations (2.23), (2.24), (2.27), and (2.28) together with (2.63) yields the equation for the temperature T listed in (3.4) below with (2.62) yielding the moisture equation. The momentum equations for $\bar{\mathbf{U}}$ and $\mathbf{U_1}$ have been derived in (2.25) and (2.26) with the parameterizations discussed above. This completes the dynamics in the simplified model.

3. Conservation Laws and Dry and Moist Phase Speeds

We begin by summarizing the final simplified equations that we have derived in the last section, the Tropical Climate Model:

$$\frac{\bar{D}\bar{\mathbf{U}}}{Dt} + \nabla \cdot (\mathbf{U_1} \otimes \mathbf{U_1}) + y\bar{\mathbf{U}}^{\perp} = -\nabla\bar{p} - \bar{d}\bar{\mathbf{U}} \tag{3.1}$$

$$\nabla \cdot \bar{\mathbf{U}} = 0 \tag{3.2}$$

$$\frac{\bar{D}\mathbf{U_1}}{Dt} + \mathbf{U_1} \cdot \nabla\bar{\mathbf{U}} + y\mathbf{U_1}^{\perp} = \nabla T - \bar{d}\mathbf{U_1} \tag{3.3}$$

$$\frac{\bar{D}T}{Dt} - \nabla \cdot \mathbf{U_1} = -d_T(T - T_{eq}) + d_{SH}(T_s - T) + P \tag{3.4}$$

$$\frac{\bar{D}q}{Dt} + \bar{Q}\nabla \cdot \mathbf{U_1} = d_q(q_s(T_s) - q) - P. \tag{3.5}$$

The form of the precipitation parameterization, P, is discussed in (2.55)-(2.61) above.

We now present several basic conservation principles for the simplified dynamics equations. For simplicity, set $\bar{d} = d_T = d_q = d_{SH} = 0$. Generalizing to the cases with the source terms is trivial, and simply adds source terms to the conservation laws. First, there is a principle of conservation of moist static energy $m = q + T$. This is given by

$$\frac{\bar{D}m}{Dt} - (1 - \bar{Q})\nabla \cdot \mathbf{U_1} = 0. \tag{3.6}$$

There is a physical justification for this equation which involves the assumed vertical gradients of humidity and buoyancy. In the nondimensional Boussinesq equations, we have assumed a mean vertical gradient for T of slope 1. Further, there is a mean gradient of q of slope $-\bar{Q}$, as explained in section 2.3.4 above. The vertical motion is

$w = -\nabla \cdot \mathbf{U_1}$ in our single mode approximation. The second term in (3.6) can therefore be understood as the vertical advection of the mean moist static energy gradient.

Another conservation principle can be obtained by eliminating the divergence terms between (3.4) and (3.5). This can be obtained by considering the quantity $q + \bar{Q}T$ which satisfies

$$\frac{\bar{D}(q+\bar{Q}T)}{Dt} = -(1-\bar{Q})P. \tag{3.7}$$

Since the precipitation P is non-negative, we have

$$\frac{\bar{D}(q+\bar{Q}T)}{Dt} \leq 0 \tag{3.8}$$

provided $0 < \bar{Q} < 1$. We will confirm later that $\bar{Q}$ must indeed be within these bounds for well-posedness.

3.1. Dissipation of Total Energy.   We now form an energy principle using this system of equations and show that this quadratic quantity is dissipated.

The total dry energy density is given by the following:

$$\epsilon_d = \frac{1}{2}(|\bar{\mathbf{U}}|^2 + |\mathbf{U_1}|^2 + T^2) \tag{3.9}$$

with the energy principle

$$\frac{\bar{D}\epsilon_d}{Dt} = -\nabla \cdot (\bar{\mathbf{U}} \cdot (\mathbf{U_1} \otimes \mathbf{U_1})) - \nabla \cdot \bar{\mathbf{U}}\bar{p} + \nabla \cdot \mathbf{U_1}\mathbf{T} + TP. \tag{3.10}$$

In this form, precipitation does work on or against the fluid depending on the sign of the temperature. We anticipate that precipitation will be a dissipative mechanism on the overall energy budget including moisture. We observe from equation (3.7) above that

$$\frac{\bar{D}}{Dt}\left(\frac{1}{2}\frac{(q+\bar{Q}T)^2}{(1-\bar{Q})(\alpha+\bar{Q})}\right) = -(\frac{\bar{Q}T+q}{\alpha+\bar{Q}})P. \tag{3.11}$$

Thus, we introduce a moist energy density contribution:

$$\epsilon_m = \frac{1}{2}\frac{(q+\bar{Q}T)^2}{(1-\bar{Q})(\alpha+\bar{Q})}. \tag{3.12}$$

Note that $\epsilon_m \geq 0$ provided $0 < \bar{Q} < 1$. Further, the addition of equation (3.10) to (3.11) will cancel the indefinite flux term and replace it by the term $-\frac{q-\alpha T}{\alpha+\bar{Q}}P$. According to the structure of the precipitation assumed in (2.55)-(2.61), $(q-\alpha T)P \geq 0$ so that this additional source term is always negative.

Thus consider the total energy density $\epsilon = \epsilon_d + \epsilon_m$. We have the local energy principle

$$\frac{\bar{D}\epsilon}{Dt} = -\nabla \cdot (\bar{\mathbf{U}} \cdot (\mathbf{U_1} \otimes \mathbf{U_1})) - \nabla \cdot (\bar{\mathbf{U}}\bar{p}) + \nabla \cdot (\mathbf{U_1}T) - \frac{q-\alpha T}{\alpha+\bar{Q}}P \tag{3.13}$$

and by integrating, we obtain the Energy Dissipation Identity

$$\int \epsilon(t)dxdy = \int \epsilon(0)dxdy - \int_0^t \int \frac{q-\alpha T}{\alpha+\bar{Q}}Pdxdydt. \tag{3.14}$$

In particular, there is decay of the total energy in the absence of forcing due to the weak dissipative effects of moisture at large scales independent of the relaxation time τ_c:

$$\int \epsilon(t)dxdy \leq \int \epsilon(0)dxdy. \tag{3.15}$$

3.2. Derivative Formulation. We can derive additional important results by considering the system formed by taking the gradient of the equations (3.1)-(3.5) above, without the barotropic mode. As mentioned earlier in 2.3.2, the approximation without the barotropic mode is often used in the simplest tropical climate model and is trivially always satisfied in one horizontal space dimension. We call this the derivative formulation, and we will derive a conservation law for this, and use it to demonstrate mean square boundedness of the first derivative within this system. One must neglect the barotropic mode ($\bar{\mathbf{U}}$) in order to derive this since the barotropic-baroclinic nonlinear transfer term makes the derivation below invalid.

Setting the barotropic velocity equal to zero in equations (3.1)-(3.5) without the forcing gives

$$\frac{\partial u_1}{\partial t} = yv_1 + \frac{\partial T}{\partial x} \tag{3.16}$$

$$\frac{\partial v_1}{\partial t} = -yu_1 + \frac{\partial T}{\partial y} \tag{3.17}$$

$$\frac{\partial T}{\partial t} = (\nabla \cdot \mathbf{U_1}) + P \tag{3.18}$$

$$\frac{\partial q}{\partial t} = -\bar{Q}(\nabla \cdot \mathbf{U_1}) - P. \tag{3.19}$$

The gradient system is then the following:

$$\frac{\partial \nabla u_1}{\partial t} = y\nabla v_1 + v_1\hat{\mathbf{e}_2} + \frac{\partial \nabla T}{\partial x} \tag{3.20}$$

$$\frac{\partial \nabla v_1}{\partial t} = -y\nabla u_1 - u_1\hat{\mathbf{e}_2} + \frac{\partial \nabla T}{\partial y} \tag{3.21}$$

$$\frac{\partial \nabla T}{\partial t} = \nabla(\nabla \cdot \mathbf{U_1}) + \nabla P \tag{3.22}$$

$$\frac{\partial \nabla q}{\partial t} = -\bar{Q}\nabla(\nabla \cdot \mathbf{U_1}) - \nabla P. \tag{3.23}$$

The dry energy flux equation for this system, analogous to equation (3.10), is given by

$$\frac{\partial \epsilon_{x,d}}{\partial t} = \frac{\partial}{\partial x}(\nabla u_1 \cdot \nabla T) + \frac{\partial}{\partial y}(\nabla v_1 \cdot \nabla T) + v_1\frac{\partial u_1}{\partial y} - u_1\frac{\partial v_1}{\partial y} + \nabla P \cdot \nabla T \tag{3.24}$$

where

$$\epsilon_{grad,d} = \frac{1}{2}(|\nabla \mathbf{U_1}|^2 + |\nabla T|^2). \tag{3.25}$$

We have a similar moist energy contribution as in the previous system (see equation (3.12)):

$$\epsilon_{grad,m} = \frac{1}{2}\frac{(\nabla q + \bar{Q}\nabla T)^2}{(1-\bar{Q})(\alpha+\bar{Q})} \tag{3.26}$$

such that setting the total energy to

$$\epsilon_{grad} = \epsilon_{grad,d} + \epsilon_{grad,m} = \frac{1}{2}\left(|\nabla \mathbf{U_1}|^2 + |\nabla T|^2 + \frac{(\nabla q + \bar{Q}\nabla T)^2}{(1-\bar{Q})(\alpha+\bar{Q})}\right) \tag{3.27}$$

gives the energy principle:

$$\frac{\partial \epsilon_{grad}}{\partial t} = \frac{\partial}{\partial x}(\nabla u_1 \cdot \nabla T) + \frac{\partial}{\partial y}(\nabla v_1 \cdot \nabla T)$$
$$+ v_1 \frac{\partial u_1}{\partial y} - u_1 \frac{\partial v_1}{\partial y} - \nabla P \cdot (\nabla(q-\alpha T)). \tag{3.28}$$

Using the chain rule, the last term can be rewritten as

$$-\nabla P \cdot (\nabla(q-\alpha T)) = -P'|\nabla(q-\alpha T)|^2. \tag{3.29}$$

Now, it follows from (2.55) in the weak sense, or equivalently, (2.59), that P' satisfies $P' \geq 0$ so this term is negative semi-definite pointwise.

We can integrate this equation in (3.29) to obtain the energy principle

$$\int \epsilon_{grad}(t)dxdy = \int \epsilon_{grad}(0)dxdy + \int_0^t \int (v_1 \frac{\partial u_1}{\partial y} - u_1 \frac{\partial v_1}{\partial y})dxdydt$$
$$- \int_0^t \int \frac{|\nabla(q-\alpha T)|^2}{\alpha + \bar{Q}}P'dxdydt$$
$$\leq \int \epsilon_{grad}(0)dxdy + \int_0^t \int (v_1 \frac{\partial u_1}{\partial y} - u_1 \frac{\partial v_1}{\partial y})dxdydt. \tag{3.30}$$

The so-called "β-effect" terms $v_1 \frac{\partial u_1}{\partial y} - u_1 \frac{\partial v_1}{\partial y}$ can cause exponential growth. However, there is always dissipation of energy in this derivative system by precipitation, independent of the convective relaxation time τ_c, and independent of convective parameterization.

The estimate in (3.30) guarantees that for any finite time interval, the quantities $\nabla \mathbf{U_1}$, ∇T, and ∇q are bounded in L^2 for bounded initial conditions independent of relaxation time. By Sobolev's Lemma, this means that smooth initial conditions cannot develop discontinuities in $\mathbf{U_1}, T, q$ in a single space dimension.

REMARK 3.1. *Since the second derivative of precipitation with respect to the saturation deficit P'' is no longer sign definite, there are no higher order energy principles. Therefore, it is natural to expect that discontinuities in the gradients of velocity, temperature, and humidity, and discontinuities in precipitation, can develop in time from appropriate smooth initial conditions in the limit of $\tau_c \to 0$.*

4. The Free Boundary Problem in the Formal Limit of Vanishing Relaxation Time

We now consider the formal limit $\tau_c \to 0$, that is, instantaneous convective adjustment. This is known as the "strict quasi-equilibrium limit" [11] since convection is assumed to keep the moisture or CAPE in a state of quasi-equilibrium (depending on our convective parameterization). Since the estimates that we derived in sections 3.1 and 3.2 above are independent of τ_c, we are assured that, at least formally, even in this limit the equations will be well-posed.

Let $\tau_c = \delta$. The moisture equation then becomes

$$\frac{\bar{D}q}{Dt} + \bar{Q}\nabla \cdot \mathbf{U_1} = d_q(q_s - q) - \delta^{-1}(q - \tilde{q}(T))^+. \tag{4.1}$$

The term of order δ^{-1} tells us that to leading order,

$$(q - \tilde{q}(T))^+ = 0. \tag{4.2}$$

Therefore the dry region Ω_d, defined as the region where there is no precipitation so $P = 0$, is given by either

$$q < \tilde{q}(T) \tag{4.3}$$

or

$$q = \tilde{q}(T), \frac{\partial q}{\partial t} \leq 0. \tag{4.4}$$

The formal limit of (4.1) in the moist region, Ω_m, where precipitation occurs and $P > 0$, is given by the constraint

$$q = \tilde{q}(T), \frac{\partial q}{\partial t} > 0. \tag{4.5}$$

With (4.2), the latter constraint, which assures that the precipitation is positive, is equivalent to

$$\frac{\partial q}{\partial t} = -\bar{\mathbf{U}} \cdot \nabla q - \bar{Q}\nabla \cdot \mathbf{U_1} + d_q(q_s - q) > 0. \tag{4.6}$$

Clearly the boundaries between Ω_d and Ω_m can change in time; they are free boundaries. Some physical mechanisms to change these boundaries include the following:

- A moist region develops places with $\nabla \cdot \mathbf{U_1} > 0$, i.e., strong enough low-level divergence to overcome evaporation and become unsaturated.
- A dry region develops a region of strong convergence with $\nabla \cdot \mathbf{U_1} < 0$, creating moisture there.
- Barotropic advection of drier air, i.e., $\bar{\mathbf{U}} \cdot \nabla q$, with $q < \tilde{q}(T)$.
- Rossby waves or Kelvin waves entrain or detrain a moist region and influence it (see [24]).

Some elementary numerical solutions demonstrating all of these physical effects are reported in [19].

4.1. Dry and Moist Waves and Free Boundaries.   The behavior of linear disturbances in our system is vastly different for saturated and unsaturated perturbations. To illustrate this in a simple context, we examine the unforced equations without the barotropic mode, equations (3.16) to (3.19). For dry (subsaturated) waves, $P = 0$ so we obtain, from equations (3.16) to (3.18)

$$\frac{\partial \mathbf{U_1}}{\partial t} + y\mathbf{U_1}^\perp - \nabla T = 0 \tag{4.7}$$

$$\frac{\partial T}{\partial t} - (\nabla \cdot \mathbf{U_1}) = 0. \tag{4.8}$$

These are the well-studied linear two-layer equatorial β-plane equations (see [13] or [24] for complete description of this set of equations and the waves therein). These equations support many interesting types of waves including equatorial Kelvin waves, Rossby waves, and mixed Rossby-gravity waves. The Kelvin wave, for instance, is symmetric about the equator, has $T = -u_1$, and propagates with speed $c_d = 1$ (in our nondimensional units).

However, for moist (saturated) disturbances, the precipitation is an important term, and we need to form the moist static energy equation to evaluate the role of disturbances. This is obtained by adding equations (3.18) and (3.19) to obtain

$$\frac{\partial(q+T)}{\partial t} - (1 - \bar{Q})\nabla \cdot \mathbf{U_1} = 0. \tag{4.9}$$

Since $q = \hat{q} + \alpha T$ for saturated disturbances, this can be written as

$$\frac{\partial T}{\partial t} - \frac{(1 - \bar{Q})}{(1 + \alpha)}\nabla \cdot \mathbf{U_1} = 0. \tag{4.10}$$

When this equation is combined with the baroclinic momentum equation (4.7) it is clear that the result is a wave equation with reduced propagation speeds. For instance, the Kelvin wave now propagates with speed $c_m = \sqrt{\frac{1-\bar{Q}}{1+\alpha}}$.

Theoretical studies that have used similar models (e.g., [32]) typically take values of $\bar{Q} \approx .8 - .9$, meaning $c_m \approx (.2 - .4)c_d$. This fits with observations as well; the data presented in the observational study of [30] shows clear spectral peak of dry disturbances at $\approx 50 m/s$, and a moist disturbance spectral peak at $\approx 15 m/s$ (see their Figure 15).

It is important to point out that the moist wave speeds are different for different convective parameterization criteria. Moist wave speeds are significantly faster for the fixed saturation ($\alpha = 0$) case than for the CAPE ($\alpha = 1$) case. Since $\bar{Q}$ is often chosen to produce moist wave speeds in accordance with observations, care must be taken when choosing this constant for different convective criteria.

We have shown that there is a significant gap between the propagation speeds of dry and moist disturbances. It is this fact that motivates our work below, where we study the implication of the two different wave speeds. The problem is made more complex by the fact that the free boundary between dry and moist regions evolves in time.

4.2. Precipitation Front Propagation.   For conceptual simplicity, we now consider the one-dimensional version of this system, which represents flow in the zonal direction around the equator. This simplification is meaningful as a first approximation because much of the important dynamics in the tropics occurs in the zonal direction, including the Walker circulation, propagation of superclusters, and the Madden-Julian Oscillation. However, the dynamics we study here can easily be extended to the 2-dimensional equatorial longwave approximation, or to the full 2-dimensional system (see [24] Chap. 9).

With this approximation, we need not consider the Coriolis force, which is dominant in midlatitudes but disappears on the equator. Further, the only appropriate value for the barotropic velocity $\bar{\mathbf{U}}$ is a constant over the domain, which we denote

by $\bar{u}$. The nondimensional equations for this system are therefore

$$\frac{\partial u}{\partial t} + \bar{u}\frac{\partial u}{\partial x} = \frac{\partial T}{\partial x} - \bar{d}u \tag{4.11}$$

$$\frac{\partial T}{\partial t} + \bar{u}\frac{\partial T}{\partial x} = \frac{\partial u}{\partial x} - d_T(T - T_{eq}) + d_{SH}(T_s - T) + \frac{(q - \tilde{q}(T))^+}{\tau_c} \tag{4.12}$$

$$\frac{\partial q}{\partial t} + \bar{u}\frac{\partial q}{\partial x} = -\bar{Q}\frac{\partial u}{\partial x} + d_q(q_s - q) - \frac{(q - \tilde{q}(T))^+}{\tau_c} \tag{4.13}$$

where u is now the zonal (eastward in the lower layer) first baroclinic mode velocity (we have dropped the subscript "1" now since this is the only dynamic velocity now) and all other variables are the same. Another important relation is the vertical velocity equation from (2.24) above which becomes

$$w = -u_x. \tag{4.14}$$

We have shown in section 3.2 that while discontinuities in q, T, and u cannot form from smooth initial conditions, it is possible that discontinuities in the derivatives of these quantities (and hence vertical velocity and precipitation) can occur out of smooth initial conditions. With this fact in mind, we now investigate the dynamics of solutions with a discontinuity in these quantities under the formal limit of $\tau_c \to 0$. We call these "precipitation fronts" since there is a discontinuity in precipitation. The fields u, T, and q only have a kink in them; there is a discontinuity in u_x, T_x, and q_x.

We consider the free wave problem with no barotropic wind, that is, $\bar{u} = \bar{d} = d_q = d_T = d_{SH} = 0$:

$$\frac{\partial u}{\partial t} = \frac{\partial T}{\partial x} \tag{4.15}$$

$$\frac{\partial T}{\partial t} = \frac{\partial u}{\partial x} + P \tag{4.16}$$

$$\frac{\partial q}{\partial t} = -\bar{Q}\frac{\partial u}{\partial x} - P. \tag{4.17}$$

The derivative form of equations (4.15) to (4.17) in this limit, obtained by taking the x-derivative and substituting the vertical velocity from equation (4.14) is:

$$\frac{\partial w}{\partial t} = -\frac{\partial T_x}{\partial x} \tag{4.18}$$

$$\frac{\partial T_x}{\partial t} = -\frac{\partial w}{\partial x} + P_x \tag{4.19}$$

$$\frac{\partial q_x}{\partial t} = +\bar{Q}\frac{\partial w}{\partial x} - P_x. \tag{4.20}$$

The jump conditions for equations (4.18) to (4.20) are as follows:

$$-s[w] = -[T_x] \tag{4.21}$$

$$-s[T_x] = -[w] + [P] \tag{4.22}$$

$$-s[q_x] = +\bar{Q}[w] - [P] \tag{4.23}$$

where s is the front propagation speed and $[f] = f_+ - f_-$.

First, there exist solutions which occur entirely within the dry and moist region. For solutions within the dry region, $[P] = 0$, and therefore we can solve equations

(4.21) and (4.22) to obtain $s = \pm 1$, the dry wave speed. For fronts entirely within the moist region, we can add equations (4.22) and (4.23) and solve to obtain $s = \pm \frac{(1-\bar{Q})}{1+\alpha}$, the moist wave speed. These solutions are not surprising, as the character of the propagation is the same as for continuous disturbances. The more interesting fronts occur at the interface between dry and moist regions, where the discontinuity in precipitation causes different propagation speeds.

To allow further study of the case with fronts at the interface between dry and moist regions, we assume, without loss of generality, that the moist region is on the positive side of the $x-$axis, and the dry region is on the negative side. We can derive conditions for the movement of the interface between dry and moist regions using the moisture constraints imposed formally by (4.2)-(4.6) in a single space dimension. First, since we are saturated in the moist region, we use the convective criterion (equation (2.58)) and the continuity of q to obtain

$$q(0) = \hat{q} + \alpha T(0) \tag{4.24}$$

at the interface. Further, to stay saturated in the moist region, we need to have

$$q_{x+} = \alpha T_{x+}. \tag{4.25}$$

Then, to assure that there is no precipitation in the dry region, we require

$$q_{x-} \geq \alpha T_{x-}. \tag{4.26}$$

Now, (4.25) and (4.26) imply

$$[q_x] \leq \alpha [T_x]. \tag{4.27}$$

Finally, we can calculate the precipitation in the moist region by adding equation (4.17) to $-\alpha$ times equation (4.16) and solving to yield

$$P_+ = \frac{(\alpha + \bar{Q})}{(1+\alpha)} w_+. \tag{4.28}$$

Since this quantity must be positive, we also have

$$w_+ > 0. \tag{4.29}$$

Of course, this just means that we have rising air in the saturated region which is physically consistent. Using these constraints, we can calculate the solutions for the precipitation fronts.

PROPOSITION 4.1. *With the saturated region initially at $x > 0$ in accordance with equations* (4.24)-(4.26)*, there are 3 branches of solutions of equations* (4.21)-(4.23) *for precipitation fronts depending on the values of the jumps in the derivatives:*
- *A branch of drying fronts with wave speeds in between the dry and moist wave speeds moving into the moist region ($1 > s > (\frac{1-\bar{Q}}{1+\alpha})^{\frac{1}{2}}$).*
- *A branch of slow moistening fronts, with speeds in between the moist speed and zero propagating into the dry region ($0 > s > -(\frac{1-\bar{Q}}{1+\alpha})^{\frac{1}{2}}$).*
- *A branch of fast moistening fronts moving into the dry region with speed above the dry wave speed ($s < -1$).*

Proof. Solving the equations (4.21) to (4.23) with the constraints (4.25) to (4.28) gives the following relations:

$$s = \pm(1 - \frac{\frac{(\alpha + \bar{Q})}{(1+\alpha)} w_+}{[w]})^{\frac{1}{2}} \tag{4.30}$$

$$[T_x] = s[w] \tag{4.31}$$

$$[q_x] = (\frac{1 - \bar{Q}}{s} - s)[w]. \tag{4.32}$$

This set of equations provides a method of constructing exact solutions from arbitrary initial jumps. For instance, given a vertical velocity $[w]$, one can calculate the necessary $[T_x]$ and $[q_x]$ to produce a balanced propagating front.

We now investigate the allowed phase speeds for these waves. For real phase speeds, we must have either

$$w_- \le (1 - \frac{\alpha + \bar{Q}}{1 + \alpha})w_+ \tag{4.33}$$

or

$$w_- \ge w_+. \tag{4.34}$$

Using the contraint (4.27), the bounds on the speed of the front are then

$$1 > s > (\frac{1 - \bar{Q}}{1 + \alpha})^{\frac{1}{2}} \text{ for } w_- < 0 \tag{4.35}$$

or

$$0 > s > -(\frac{1 - \bar{Q}}{1 + \alpha})^{\frac{1}{2}} \text{ for } 0 < w_- < (1 - \frac{\alpha + \bar{Q}}{1 + \alpha})w_+ \tag{4.36}$$

or

$$s < -1 \text{ for } w_- > w_+. \tag{4.37}$$

The dry wave speed is $c_d = 1$, and the moist wave speed is $c_m = \sqrt{\frac{1 - \bar{Q}}{1 + \alpha}}$, so the above constraints can be rewritten as:

$$c_d > s > c_m \tag{4.38}$$

or

$$0 > s > -c_m \tag{4.39}$$

or

$$s < -c_d. \tag{4.40}$$

The first branch of front speeds (equation (4.35)) we call the drying front, since it propagates from the dry region into the moist region. Note that w_- is negative for these drying waves so the state adjacent to the moist region has downdrafts and

divergence at the bottom of the troposphere consistent with drying. This family of fronts exactly spans the region between dry and moist wave speeds, which is the exact range given for stability of fronts by Lax's Stability Criterion [23].

The second branch (equation (4.36)) we call the slow moistening fronts. This branch is particularly interesting because it produces movement of the interface between dry and moist at a speed that is below the moist wave speed. Note that according to (4.36), w_- is positive with low level convergence in the flow field but bounded from above by a multiple less than one of w_+; furthermore, slower waves have larger w_- in the unsaturated state. Since most models overestimate the speed of such tropical phenomena as the Madden-Julian Oscillation, this branch is perhaps the most physically interesting.

The final branch (equation (4.37)) we call the fast moistening front. This consists of moistening propagating at speeds faster than the dry wave speed. According to (4.37) and (4.14), the fast moistening occurs from large convergence in the dry region, which brings the dry region to saturation rapidly.

Note the important asymmetry between "drying waves" (with $s > 0$, that is, the precipitation front propagating into the moist region) and "moistening waves" (with $s < 0$). The moistening waves both violate Lax's stability criterion so it becomes interesting to understand their potential dynamical significance; this is a main topic in section 5.

Since the front speeds are bounded by the dry and moist wave speeds, there is no difference in allowed propagation speeds between systems with different convective criteria (i.e., different α). However, systems with the same initial discontinuities do not behave the same as α is varied, since α appears in equation (4.30). Next, we investigate the effect of finite relaxation time, as well as the effective differences among systems with different convective criteria in a numerical model. □

5. Numerical Simulation of Fronts

We now present numerical results of simulations of these fronts over a range of convective relaxation times, demonstrating that the theoretical predictions made in section 4.2 in the limit of $\tau_c \to 0$ are surprisingly accurate up to large values of the relaxation time. Even the two moistening fronts which violate Lax's Stability Criterion are readily realizable in the numerics presented below. We additionally investigate sensitivity to the convective criterion, and to the numerical mesh.

5.1. Description of Numerical Model.   We numerically simulate the one-dimensional forced-dissipative system with arbitrary relaxation time, i.e., equations (4.11) to (4.13). Since we are considering a somewhat stiff problem (with small convective relaxation times), care must be taken when designing the numerical method. First of all, by considering the quantity $Z_0 = q + \bar{Q}T$, introduced earlier in (3.7), one of the equations becomes an ODE in the absence of mean wind. Secondly, we can isolate the westward and eastward moving waves by using the characteristics $Z_E = u - T$ and $Z_W = u + T$ as variables (the subscripts represent eastward and westward propagation, respectively).

Therefore the equations we integrate are:

$$\frac{\partial Z_E}{\partial t} + \bar{u}\frac{\partial Z_E}{\partial x} + \frac{\partial Z_E}{\partial x} = -S_{T,R} - S_{T,SH} + S_u - P \tag{5.1}$$

$$\frac{\partial Z_W}{\partial t} + \bar{u}\frac{\partial Z_W}{\partial x} - \frac{\partial Z_W}{\partial x} = S_{T,R} + S_{T,SH} + S_u + P \tag{5.2}$$

$$\frac{\partial Z_0}{\partial t} + \bar{u}\frac{\partial Z_0}{\partial x} = \bar{Q}S_{T,R} + E - (1-\bar{Q})P \tag{5.3}$$
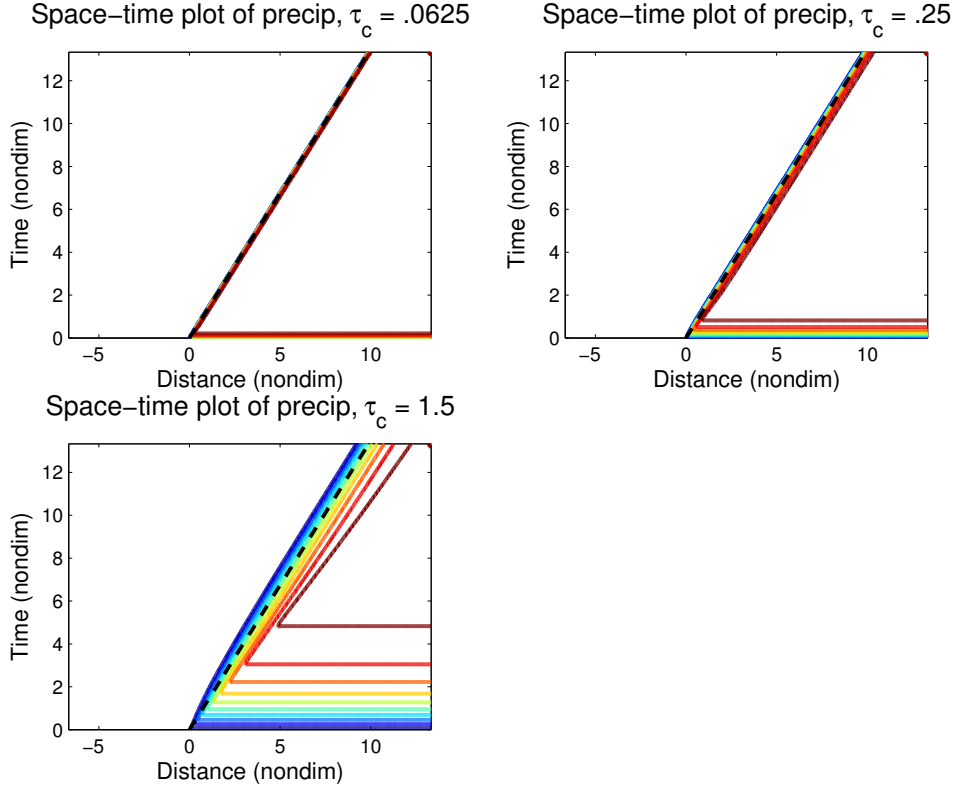
FIG. 5.1. *Space-time diagrams of precipitation for the drying front simulations.*

where $S_{T,R} = -d_T(\frac{Z_E+Z_W}{2} - T_{eq})$, $S_{T,SH} = d_{SH}(T_s - \frac{Z_E+Z_W}{2})$, $S_u = \bar{d}(\frac{Z_E-Z_W}{2})$, $E = d_q(q_s - Z_0 + \frac{\bar{Q}}{2}(Z_E+Z_W))$, and $P = \frac{(Z_0 - \frac{Q}{2}(Z_E+Z_W) - \tilde{q}(T))^+}{\tau_c}$.

For numerical integration of the scalar wave equations, we use the 3rd order ENO scheme [14] for spatial differencing. This provides a high order of accuracy, while preserving very sharp resolution near fronts with minimal numerical dissipation.

An added difficulty is that the precipitation term is stiff for small values of τ_c; essentially this term can cause unphysical oscillations, and even reduction of q below its saturation value for $\tau_c \sim \Delta t$. Therefore for time integration, we use Strang time splitting on this term, which gives 2nd order in time accuracy, and facilitates simulation of the precipitation term to small values of τ_c. The typical mesh spacing used is .0267 (40 km), so we expect the shocks to be well resolved within 100 km. We use a small time step of .0033 (100 seconds) to resolve the short-time relaxation effects.

5.2. Simulations. The basic parameters we use in the simulations below are the following:
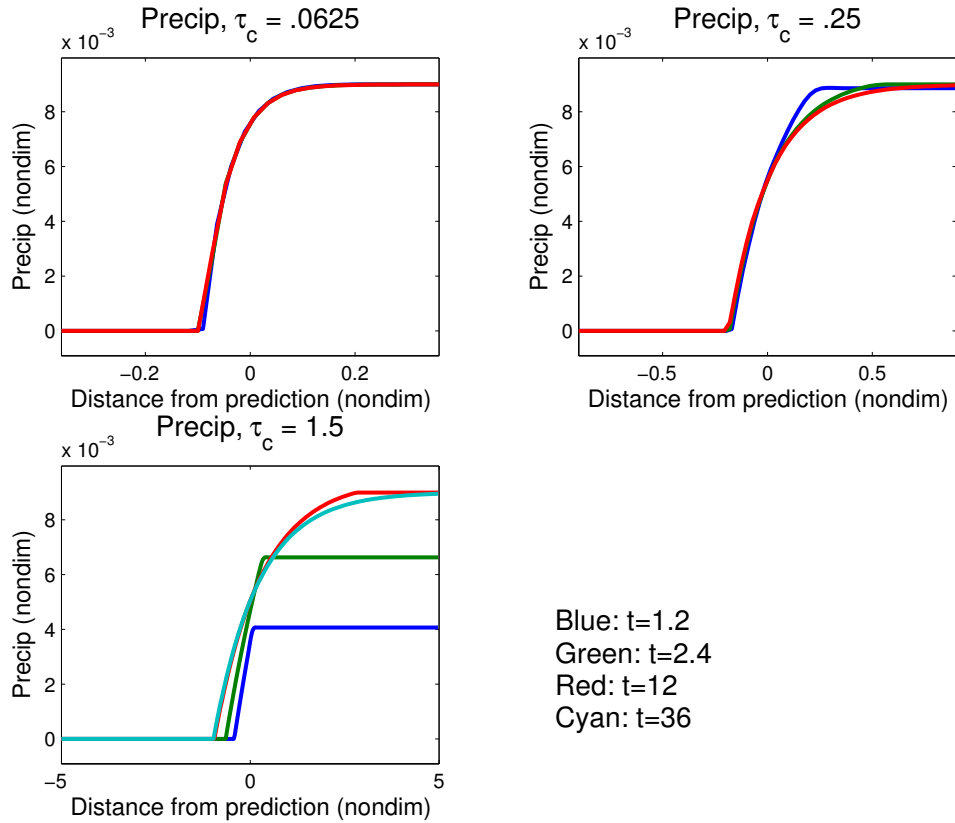
$$\bar{Q} = .9, \alpha = 0, \hat{q} = .9. \tag{5.4}$$

Fig. 5.2. *Precipitation for the drying fronts at t=1.2, t=2.4, and t=12 vs. distance recentered by the theoretical prediction for shock position. t=36 is additionally plotted for the $\tau_c = 1.5$ case. Note the different distance scales for each simulation.*

The Drying Front

We first simulate a drying front. The initial conditions for this simulation are

$$w_+ = .01 \tag{5.5}$$

$$T_{x+} = 0 \tag{5.6}$$

$$q_{x+} = 0 \tag{5.7}$$

$$w_- = -.01 \tag{5.8}$$

$$T_{x-} = -.02\sqrt{.55} = -.0148 \tag{5.9}$$

$$q_{x-} = \frac{.009}{\sqrt{.55}} = .0121 \tag{5.10}$$

which yield a balanced front with speed $s = \sqrt{.55} = .742$ in the formal limit of vanishing relaxation time. We simulate using a range of convective relaxation times: $\tau_c = .0625, .25,$ and 1.5 in nondimensional units (30 min, 2 hrs, and 12 hrs, respectively). The 12 hour relaxation time is that found in [5], 2 hours is typically used with the Betts-Miller convection scheme in general circulation models, and the 30 minute relaxation time simulations are performed to get an idea of how close we are

to the $\tau_c \rightarrow 0$ limit.

Figure 5.1 shows space-time plots of the precipitation for this drying front at the three relaxation times, along with the predicted front speed (the black dotted line in each plot). The time of simulation is $t = 13.33$, or 4.44 days in dimensional units. All simulations agree with the predicted front speed quite well, if one considers the center of the front region. The $\tau_c = .0625$ simulation is virtually identical to predictions for all time, and the front remains very abrupt. Only small deviations from the prediction can be seen for the .25 relaxation time simulation. In the simulation with $\tau_c = 1.5$, however, the front has been smoothed out quite a bit. The center of the front region still agrees with the predicted speed quite well though.
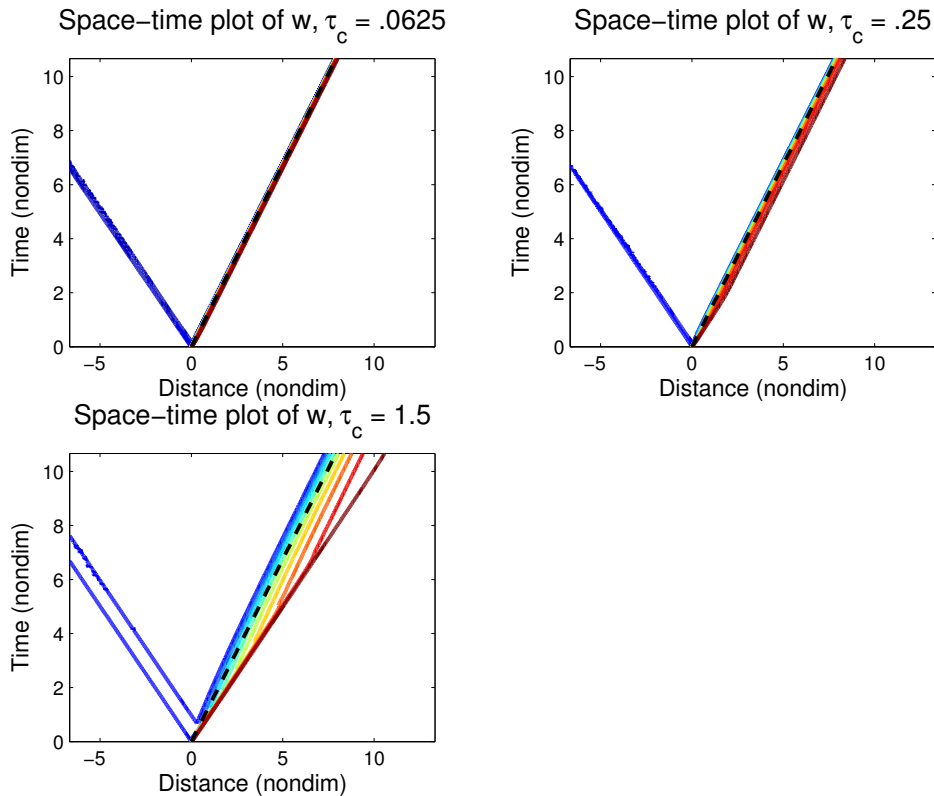
FIG. 5.3. *Space-time diagrams of vertical velocity for the drying front simulations.*

We next demonstrate that the smoothing of the front primarily occurs during the "spin-up" of the fronts, i.e., the adjustment time it takes for the precipitation to reach its proper value, and that the fronts propagate steadily after a certain time. The steady state of the precipitation in the unperturbed moist region for these cases is $P_+ = \bar{Q}w_+ = .009$, implying a steady state humidity of $q_+ = \tilde{q} + \tau_c P_+ = .9 + .009\tau_c$. Since the initial condition for the humidity begins exactly at the saturation value (.9), it takes on the order of the convective relaxation time for adjustment to this steady state to occur. As can be seen from Figure 5.1, this amount of time is approximately $2\tau_c$ for each of the simulations. The steady shapes of the precipitation profiles can be seen in Figure 5.2, which contains plots at different time slices for the three drying

fronts, shifted by the predicted speed. That is, we plot $P(x-st,t)$ for $t=1.2, t=2.4$, and $t=12$ where $s=\sqrt{.55}$, the predicted speed. There is a significant difference in distance scale for the three plots. The two smaller relaxation cases both converge to the steady profile quickly. The spinup of precipitation can be seen more clearly in the $\tau_c=1.5$ simulation, as the $t=1.2$ and $t=2.4$ slices are both in the process of adjusting. Even the $t=12$ slice is not completely at steady state for this case, so we additionally plot a time slice at $t=36$ to indicate the steady state. The simulations do not drift from these steady states once reached. Plotting the vertical velocity (Figure 5.3), one can see that there are dry waves propagating into the dry region created in the adjustment process. The fetch of these waves is proportional to the adjustment time, with the front expelling waves until approximately $t=2\tau_c$.

From these simulations we can conclude that our theory regarding the limit as $\tau_c \to 0$ can be applied to the realistic adjustment cases. The structure of the fronts are steady in the moving frame provided $t \gg \tau_c$, where t is the time over which the integration is performed.

The Slow Moistening Front We next simulate the slow moistening front, with
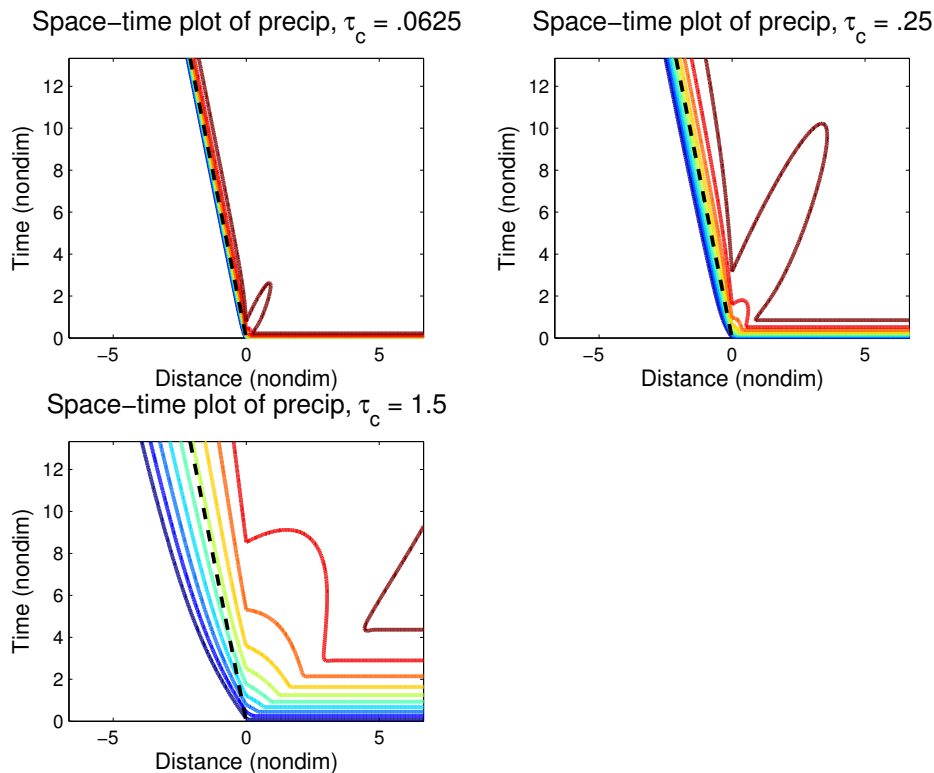

FIG. 5.4. *Space-time diagrams of precipitation for the slow moistening front simulations.*

initial conditions as follows:

$$w_+ = .01 \tag{5.11}$$

$$T_{x+} = 0 \tag{5.12}$$

$$q_{x+} = 0 \tag{5.13}$$

$$w_- = \frac{1}{1300} = .000769 \tag{5.14}$$

$$T_{x-} = \frac{3\sqrt{.1}}{650} = .00146 \tag{5.15}$$

$$q_{x-} = \frac{9\sqrt{.1}}{650} = .00438 \tag{5.16}$$

which creates a balanced front with speed $s = -\frac{\sqrt{.1}}{2} = -.158$ in the formal limit of vanishing relaxation time. The plots for this wave (Figure 5.4) are given for the same time period, $t = 13.33$, and are displayed on a slightly smaller spatial domain. Again the speeds are well-predicted by our $\tau_c \to 0$ theory, when the center of the front region is considered. However more spreading of the fronts is observed here, which again primarily occurs during the precipitation adjustment period. This is clear in the $\tau_c = .25$ simulation as well as the $\tau_c = 1.5$. For instance, the $\tau_c = 1.5$ front
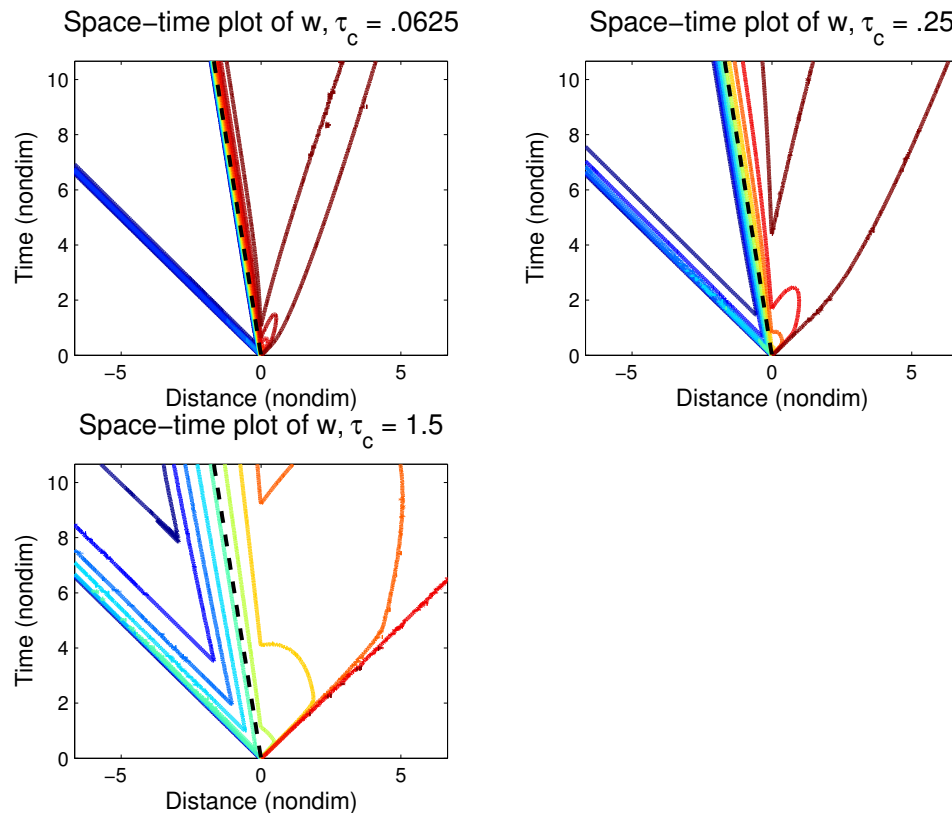

FIG. 5.5. *Space-time diagrams of vertical velocity for the moistening front simulations.*

is approximately 75% wider than the corresponding drying front in the previous case.

Examining the vertical velocities (Figure 5.5), one can see that there are now both dry waves (propagating into the dry region) and moist waves (propagating into the moist region) being emitted from the front during the adjustment phase. The influence of the moist waves can be seen in the precipitation fields in Figure 5.4. The character of the dry waves is similar to the dry waves being emitted from the drying front, i.e., propagation at the dry phase speed with width proportional to the adjustment time. The behavior of the moist waves is more complex. After an adjustment period (here approximately $t = 4\tau_c$), the moist wave simply propagates into the moist region at the moist speed. However, prior to this, the wave expands, with the boundary on the positive side moving at the dry wave speed. Propagation at speeds above the moist wave speed in precipitating regions can occur in the system where $\tau_c > 0$, since changes in divergence do not immediately affect the precipitation. Specifically, the assumption that $q = \hat{q} + \alpha T$, which we used between equations (4.9) and (4.10) in deriving the properties of moist disturbances in Section 4.1 breaks down. When the precipitation is adjusting to its steady value given a certain velocity divergence, small wave perturbations to this do not affect the evolution of the precipitation much, and hence the waves propagate more like dry disturbances.
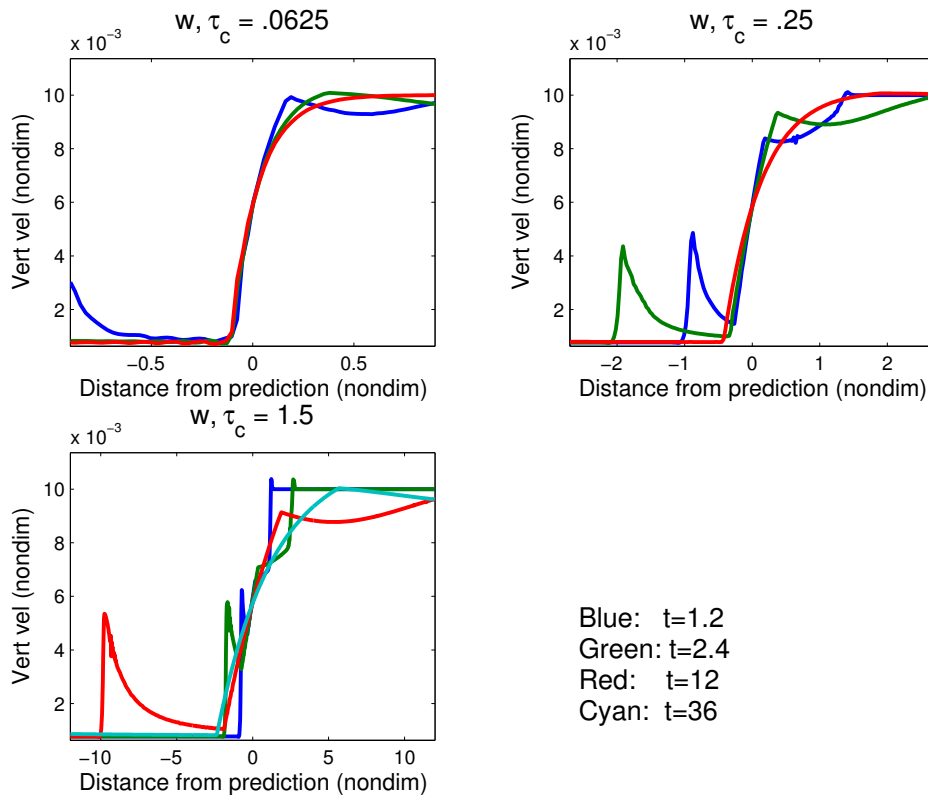

Fig. 5.6. *Vertical velocity for the slow moistening fronts at t=1.2, t=2.4, and t=12 vs. distance recentered by the theoretical prediction for shock position. t=36 is additionally plotted for the $\tau_c = 1.5$ case.*

In Figure 5.6 we plot the vertical velocities at different times, recentered by the predicted front speed. In these plots one can see the structure of the dry waves propagating away from the interface, as well as some of the moist wave propagation. Again all of these waves eventually propagate with a steady shape after a certain length of time, approximately given by the $t = 36$ plot for the $\tau_c = 1.5$ case, and the $t = 12$ plots in the shorter relaxation time cases. Keeping in mind the different spatial scales in the plots, the emerging steady states clearly retain the same smoothed shape for the two smaller relaxation times; also see figures 5.7 and 5.8 below which confirms this.

Since we believe this wave is the most interesting to the atmospheric science community (due to its reduced phase speeds), we now examine the sensitivity of these simulations to both resolution (by considering 2x and .5x resolutions) and convective parameterization (by constructing a wave with a similar propagation speed in the CAPE parameterization). First, plots similar to Figure 5.6 for double and half resolution are given in Figure 5.7 and 5.8. These plots give time slices of vertical velocity (which exhibits the largest change with resolution) for the $\tau_c = .25$ case (Fig. 5.7) and the $\tau_c = .0625$ case (Fig. 5.8). The primary difference evident in these plots is not in the fronts, which are all nearly identical, but rather with the dry waves propagating
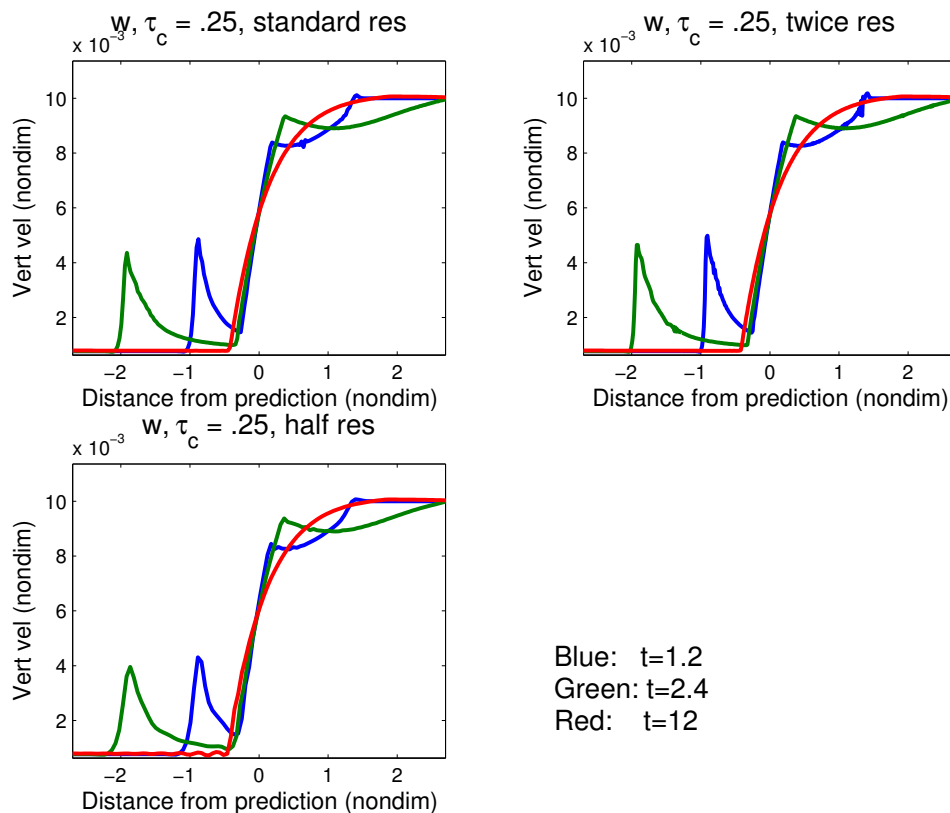

FIG. 5.7. *Testing resolution with the $\tau_c = .25$ simulation: vertical velocity with rescaled distance at t=1.2, t=2.4, and t=12.*
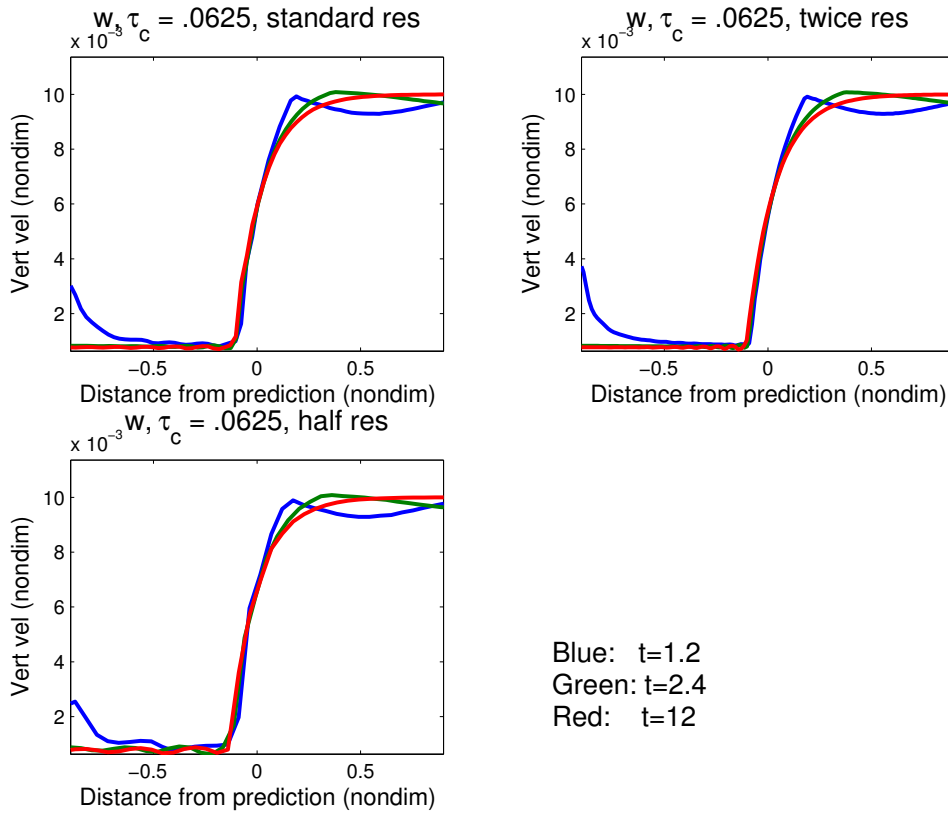
Fig. 5.8. *Testing resolution with the $\tau_c = .0625$ simulation: vertical velocity with rescaled distance at t=1.2, t=2.4, and t=12.*

away, which are slightly better defined for the cases with higher resolution. This gives us faith in the numerical simulation of the precipitation fronts however. We next consider a slow moistening front with the same speed under the CAPE parameterization ($\alpha = 1$) which is constructed by using the following values:

$$w_+ = .01 \tag{5.17}$$

$$T_{x+} = 0 \tag{5.18}$$

$$q_{x+} = 0 \tag{5.19}$$

$$w_- = \frac{1}{3900} = .000256 \tag{5.20}$$

$$T_{x-} = \frac{19\sqrt{.1}}{3900} = .00154 \tag{5.21}$$

$$q_{x-} = \frac{19\sqrt{.1}}{1300} = .00462 \tag{5.22}$$

which again gives a theoretical propagation speed of $s = -\frac{\sqrt{.1}}{2}$. Again, the theoretical prediction for the it is strikingly accurate (Figure 5.9). There is a small amount more smoothing of the front here as compared with the fixed saturation case; these fronts
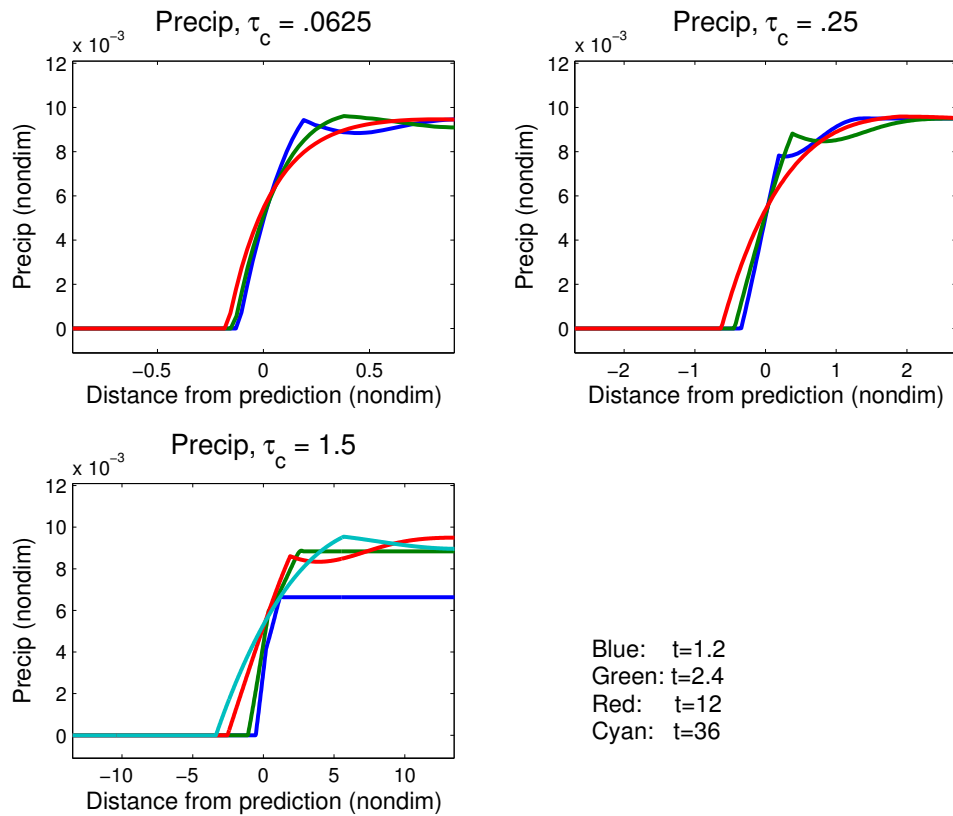
Fig. 5.9. *Precipitation for the slow moistening fronts with the CAPE parameterization at t=1.2, t=2.4, and t=12 vs. distance recentered by the theoretical prediction for shock position. t=36 is additionally plotted for the $\tau_c = 1.5$ case.*

also take slightly longer to reach steady state (despite the fact that the precipitation adjusts faster in the $\tau_c = 1.5$ case). Other than these observations, the shape of the fronts, the character of the propagation, and the agreement with theoretical predictions are similar to the cases with $\alpha = 0$.

The Fast Moistening Front

Finally we simulate the fast moistening front, with the following initial conditions:

$$w_+ = .01 \tag{5.23}$$
$$T_{x+} = 0 \tag{5.24}$$
$$q_{x+} = 0 \tag{5.25}$$
$$w_- = .013 \tag{5.26}$$
$$T_{x-} = -.006 \tag{5.27}$$
$$q_{x-} = .00585 \tag{5.28}$$

which gives a speed of $s = -2$ in the formal limit of vanishing relaxation time. In Figure 5.10, we plot time slices of the precipitation for the three values of τ_c for this case. Despite its predicted propagation of twice the dry wave speed, this wave
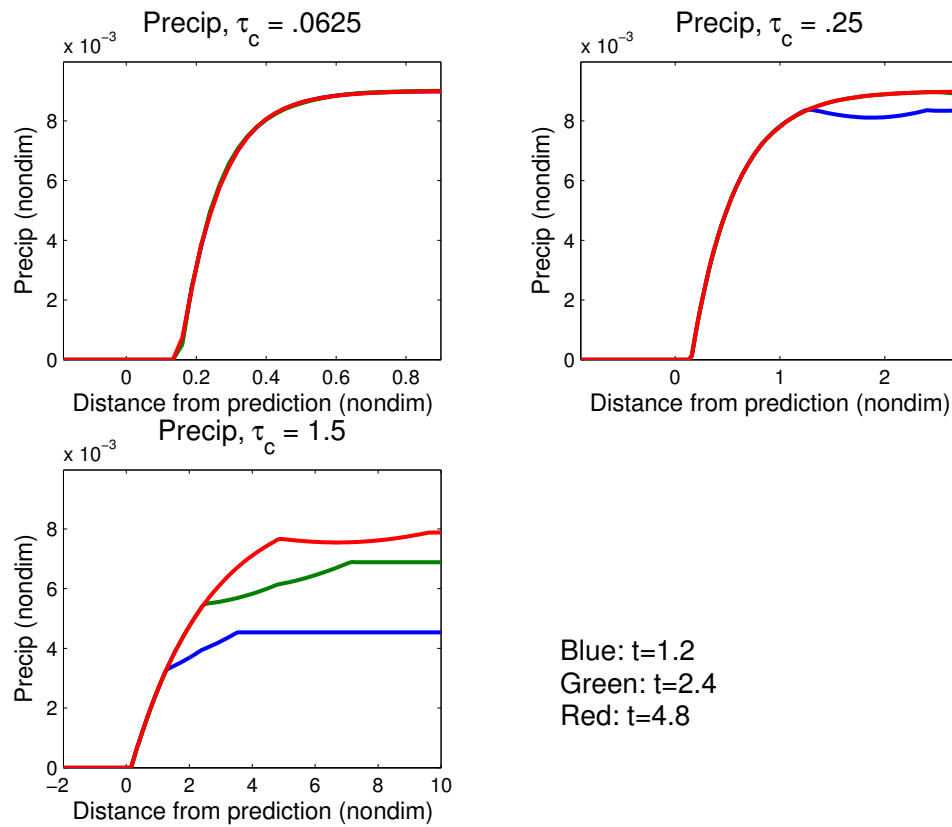
Fig. 5.10. *Precipitation for the fast moistening fronts at t=1.2, t=2.4, and t=12 vs. distance recentered by the theoretical prediction for shock position.*

is still realizable numerically, and the theoretical predictions are still quite accurate for all three cases. The primary difference from other simulations is that the waves lag behind the theoretical predictions in all three cases due to a phase shift in the adjustment process. This is not surprising since the front propagation speed is faster than any allowed characteristic wave speed; while the precipitation is ramping up to its steady value, the front falls behind the theoretical prediction. The waves still reach a steady state in the moist reference state in this case, though, which is similar to the other cases. The lags, measured by the location of half maximum, are approximately .2, .5, and 2 for $\tau_c = .0625, .25$, and 1.5, respectively. The waves actually reach their steady shape more quickly in this case than for the drying and slow moistening fronts.

REMARK 5.1. *The three branches of precipitation fronts, drying, slow and fast moistening, are reminiscent of the three branches of wave fronts in reacting gas flow, strong detonations, flame fronts, and weak detonations [41] which satisfy the analogous wave speed bounds in* (4.38), (4.39), (4.40), *respectively. In combustion the strong detonations, which satisfy Lax's shock inequalities as in* (4.38) *are always realizable ([22]; [4]) while flame fronts satisfying* (4.39) *propagate at speeds that are determined as a nonlinear eigenvalue problem through a subtle balance of reaction and diffusion [41];*

weak detonations satisfying (4.40) are even more elusive and hard to realize ([22]; [8]) with special values of diffusion rates needed. The numerical results just presented for precipitation fronts show that for the atmospheric models considered here, all three types of precipitation fronts are realizable as large time limits for any finite relaxation time τ_c with only finite one-sided relaxation as a subtle damping mechanism and with negligible dependence on (numerical) diffusion coefficients. One significant difference in the behavior of the system studied in section 4 is that the basic jump discontinuities occur in the first derivatives of the solution while the nonlinear source terms involve the smoother integrals involving values of the functions themselves; thus, the finite time relaxation effects create a relatively smoother and thus more realizable background environment for the propagation of discontinuities in first derivatives. This is not the case in reacting gas flow where both the nonlinear source terms and the discontinuities occur at the level of primitive variables such as temperature.

6. 1-Dimensional Walker Cell Solutions

The Walker Cell is the zonal circulation of the atmosphere at the equator. Over the warmest sea surface temperatures in the western Pacific Ocean "warm pool," air rises, and subsides in areas of colder sea surface temperatures; this flow is the Walker Circulation. We model this with the 1-D forced-dissipative system (equations (4.11) to (4.13)) by setting up sample sea surface temperature distributions representing the warm pool (the parameter q_s in the evaporation parameterization), and simulating the precipitation response, integrated to a steady state, over a periodic domain all the way around the equator.

We show in this section that even over smooth sea surface temperature distributions, discontinuities in precipitation can develop in this Walker cell model, which provides further physical justification for our study of precipitation fronts in the previous sections. We begin by analyzing what is required to create a discontinuity in precipitation in this model for steady states in the limit of $\tau_c \to 0$.

Solutions in the Limit of $\tau_c \to 0$

The equations we analyze formally below are the steady state of equations (4.11) to (4.13):

$$\bar{u}\frac{\partial u}{\partial x} = \frac{\partial T}{\partial x} - \bar{d}u \tag{6.1}$$

$$\bar{u}\frac{\partial T}{\partial x} = \frac{\partial u}{\partial x} - d_T(T - T_{eq}) + d_{SH}(T_s - T) + P \tag{6.2}$$

$$\bar{u}\frac{\partial q}{\partial x} = -\bar{Q}\frac{\partial u}{\partial x} + d_q(q_s - q) - P \tag{6.3}$$

where $P = \frac{(q - \bar{q}(T))^+}{\tau_c}$ in the limit of $\tau_c \to 0$. Our reasoning below is somewhat formal but instructive. From the moisture equation (6.3), we obtain

$$P = d_q(q_s - q) - \bar{Q}\frac{\partial u}{\partial x} - \bar{u}\frac{\partial q}{\partial x}. \tag{6.4}$$

For there to be a discontinuity in P, there must be a corresponding discontinuity in at least one of these three terms. As we showed in section 3.2, discontinuities in q, T, or u cannot occur out of smooth initial conditions and we assume that the steady state in (6.1)-(6.3) arises formally as the large time asymptotic limit from smooth initial data for each τ_c. Therefore the discontinuity must be from either the second or third term in the above, i.e., either $\frac{\partial u}{\partial x}$ or $\frac{\partial q}{\partial x}$ must be discontinuous for P to be discontinuous.

This also implies that in the absence of mean wind ($\bar{u}=0$), P is discontinuous if and only if $\frac{\partial u}{\partial x}$ is also discontinuous.

Now consider the moist static energy equation derived from adding equations (6.2) and (6.3) (this eliminates the precipitation term):

$$\bar{u}\frac{\partial(T+q)}{\partial x} = (1-\bar{Q})\frac{\partial u}{\partial x} + d_q(q_s-q) - d_T(T-T_{eq}) + d_{SH}(T_s-T) + d_q(q_s-q) \quad (6.5)$$

In the case where $\bar{u}=0$, one can solve for $\frac{\partial u}{\partial x}$ as a function of continuous variables only. Therefore with no mean wind, there can be no discontinuity in precipitation. With mean wind, there is no such guarantee, and discontinuities are possible.

[6] discusses the variation of the Walker cell with sea surface temperature gradients in a model similar to ours (essentially a 1-D version of the QTCM). They observe that in their model, nonlinear advection of moisture is key for the presence of precipitation discontinuities. Since they use no linear advection by mean wind, this is obviously connected to the result above.

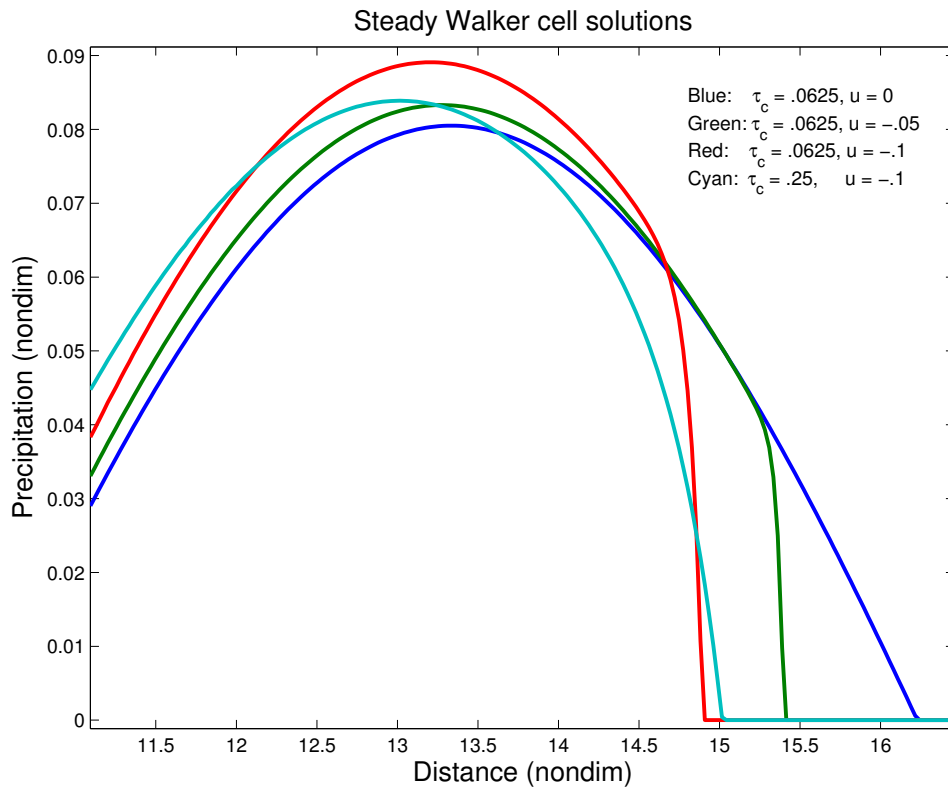**6.1. Numerical Results.**   We simulate steady Walker cell solutions using the

FIG. 6.1. *Steady Walker cell solutions, $\tau_c = .0625$ and $\bar{u}=0$ (blue); $\tau_c = .0625$ and $\bar{u}=-.05$ (green); $\tau_c = .0625$ and $\bar{u}=-.1$ (red); $\tau_c = .25$ and $\bar{u}=-.1$ (cyan).*

following parameters:

$$\bar{Q}=.9, \alpha=0, \hat{q}=.9, d_{SH}=0, d_q=\frac{1}{24}, d_T=\frac{1}{48}, \bar{d}=0, T_{eq}=-.6 \quad (6.6)$$

We vary the convective relaxation time τ_c and the mean wind $\bar{u}$ in the following simulations. The distribution of q_s is the following:

$$q_s = \begin{cases} 1.1 & \text{for } 0 < x < \frac{3}{8}R_E \text{ and } \frac{5}{8}R_E < x < R_E, \\ 1.1 + .26sin\left(\frac{4\pi}{R_E}(x - \frac{3}{8}R_E)\right) & \text{for } \frac{3}{8}R_E < x < \frac{5}{8}R_E, \end{cases}$$

(6.7)

which represents a sea surface temperature perturbation of 3K over the warm pool (one-fourth of the domain) with $R_E = 26.67$, the Earth's circumference.

Figure 6.1 contains simulations with $\tau_c = .0625$ (30 minutes) using this distribution of q_s, varying mean wind from 0 to $-.09$. There is additionally one simulation with $\tau_c = .25$ and $\bar{u} = -.09$. The upper limit mean wind (4.5 m/s) is still within realistic values of the mean easterly winds at the equator. Clearly, for each of the simulations with small τ_c and mean winds, the precipitation distribution is approximately discontinuous. The simulation with no mean wind is smooth as expected. However, the simulation with larger τ_c is not nearly as abrupt in transition as the simulations with smaller τ_c. These simple simulations demonstrate that the concept of precipitation front developed in sections 4 and 5 is useful and realizable even for steady state solutions with realistic damping.

7. Some Future Directions in Applied Analysis for Large Scale Precipitation Dynamics

From the viewpoint of tropical atmospheric dynamics, the theory developed here provides a new perspective on the fashion in which the prominent large scale zones of moisture in the tropics can move and interact with large scale dynamics in the quasi-equilibrium approximation through novel hyperbolic free boundary problems. Some of these applied aspects are developed elsewhere by the authors ([35], [19]). The style of this paper involves concise formal analysis and new estimates rather than rigorous proofs in the style of applied analysis. The work presented above suggests several interesting problems for rigorous applied analysis in a remarkable new PDE system with subtle damping effects, the Tropical Climate Model in (3.1)-(3.5) of section 3. We list some of them briefly below.

Qualitative Behavior

- Classify all smooth initial data for the relaxation limit free boundary problem discussed in section 4.2 which develop discontinuities in finite time in temperature gradients, vertical motion, and precipitation. Include the effects of damping and forcing described earlier.
- As discussed in section 6, classify all the steady states for the relaxation limit free boundary problem which have discontinuous precipitation zones arising from smooth imposed sea surface temperature distributions.
- The same problem as above for the Tropical Climate Model in (3.1)-(3.5) without and with the barotropic flow.
- Study the existence and structure of traveling waves for the 1-D equations in (4.15)-(4.17) for finite relaxation times τ_c and for the three types of precipitation fronts in section 4.2. How much does the structure of this smoothed traveling wave reflect the nature of the precipitation front and the structure of the convective parameterization as presented through the parameter α? When is the adjustment problem for finite τ_c dynamically stable?

Quantitative Behavior

- For the version of the Tropical Climate Model without barotropic flow, the estimates for solutions and first derivatives allow one to pass to the limit of vanishing relaxation times. With the above estimates, characterize the weak solutions of the associated hyperbolic free boundary problem through variational inequalities [20] and establish their uniqueness. When is there additional partial regularity?
- Establish the same results as in the above for the complete Tropical Climate Model including barotropic flow. Here a new estimate beyond those in section 3 independent of τ_c is needed for the quadratically nonlinear barotropic-baroclinic coupling.
- For a given steady state surface forcing distribution and damping as in section 6, develop a theory for the weak attractor at large times for finite τ_c. Can this attractor include multiple steady states, periodic orbits, chaotic dynamics?
- The same issues as in the above, for the two-dimensional Tropical Climate Model without (and with) barotropic flow coupling.

One of the authors (A.M.) plans to investigate some of these issues with collaborators in the near future. The reader is invited to make progress on these interesting issues for applied analysis.

REFERENCES

[1] Arakawa, A. and W. H. Schubert, *Interaction of a cumulus cloud ensemble with the large-scale environment, Part I.* J. Atmos. Sci., 31, 674-701, 1974.

[2] A. K. Betts, *A new convective adjustment scheme, Part I: Observational and theoretical basis*, Quart. J. Roy. Meteor. Soc., 112, 677-692, 1986.

[3] A. K. Betts and M. J. Miller, *A new convective adjustment scheme, Part II: Single column tests using GATE wave, BOMEX, and arctic air-mass data sets*, Quart. J. Roy. Meteor. Soc., 112, 693-709, 1986.

[4] A. Bourlioux and A. J. Majda, *Theoretical and numerical structure of unstable detonations*, Phil. Trans. R. Soc. London A, 350, 29-68, 1995.

[5] C. S. Bretherton, M. E. Peters and L. E. Back, *Relationships between water vapor path and precipitation over the tropical oceans*, J. Climate, 17, 1517-1528, 2004.

[6] C. S. Bretherton, and A. H. Sobel, *A simple model of a convectively coupled Walker Circulation using the weak temperature gradient approximation*, J. Climate, 15, 2907-2920, 2002.

[7] G. Q. Chen, C. D. Levermore and T. P. Liu, *Hyperbolic conservation laws with stiff relaxation terms and entropy*, Comm. Pure Appl. Math., 47, 787-830, 1994.

[8] P. Colella, A. Majda and V. Roytburd, *Theoretical and numerical structure for reacting shock waves*, SIAM J. Sci. Statist. Comput., 7, 1059-1080, 1986.

[9] K. A. Emanuel, *An air-sea interaction model of intraseasonal oscillations in the tropics*, J. Atmos. Sci., 44, 2324-2340, 1987.

[10] K. A. Emanuel, *An air-sea interaction model of intraseasonal oscillations in the tropics*, Atmospheric Convection, Oxford Press, 1994.

[11] K. A. Emanuel, J. D. Neelin and C. S. Bretherton, *On large-scale circulations in convecting atmospheres*, Quart. J. Roy. Meteor. Soc., 120, 1111-1143, 1994.

[12] A. E. Gill, *Some simple solutions for heat-induced tropical circulation*, Quart. J. Roy. Meteor. Soc., 106, 447-462, 1980.

[13] A. E. Gill, *Atmosphere-Ocean Dynamics*, Academic Press, 1982.

[14] A. Harten, B. Engquist, S. Osher and S. R. Chakravarthy, *Uniformly high order accurate essentially non-oscillatory schemes III*, J. Comput. Phys., 71, 231-303, 1987.

[15] D. L. Hartmann, *Global Physical Climatology*, Academic Press, 1994.

[16] I. M. Held and I.-S. Kang, *Barotropic models of the extratropical response to El Niño*, J. Atmos. Sci., 44, 3576-3586, 1987.

[17] S. Jin and Z. P. Xin, *The relaxation schemes for systems of conservation laws in arbitrary space dimensions*, Comm. Pure Appl. Math., 48, 235-276, 1995.

[18] M. A. Katsoulakis and A. E. Tzavaras, *Contractive relaxation systems and the scalar multidimensional conservation law*, Comm. Partial Diff. Eqns., 22, 195-233, 1997.

[19] B. Khouider and A. J. Majda, *A high resolution balanced scheme for an idealized tropical climate model*, Submitted to Theoret. and Comp. Fluid Dyn., 2004.

[20] D. Kinderlehrer and G. Stampacchia, *An Introduction to Variational Inequalities and Their Applications*, Academic Press, 1980.

[21] R. A. Madden and P. Julian, *Observations of the 40-50 day tropical oscillation- A review*, Mon. Wea. Rev., 122, 814-837, 1994.

[22] A. J. Majda, *A qualitative model for dynamic combustion*, SIAM J. Appl. Math., 41, 70-93, 1981.

[23] A. J. Majda, *Compressible Fluid Flow and Systems of Conservation Laws In Several Space Variables*, Applied Math. Sciences 53, Springer-Verlag, New York, 1984.

[24] A. J. Majda, *Introduction to PDE's and Waves for The Atmosphere and Ocean*, Courant Institute Lecture Series #9, Amer. Math. Soc., 2003.

[25] A. J. Majda and J. A. Biello, *The nonlinear interaction of barotropic and equatorial baroclinic Rossby waves*, J. Atmos. Sci., 60, 1809-1821, 2003.

[26] A. J. Majda, B. Khouider, G. Kiladis, K. Straub and M. Shefter, *A model for convectively coupled tropical waves: nonlinearity, rotation and comparison with observations*, in press, J. Atmos. Sci., 2004.

[27] A. J. Majda and M. Shefter, *Models of stratiform instability and convectively coupled waves*, J. Atmos. Sci., 58, a, 1567-1584, 2001.

[28] A. J. Majda and M. Shefter, *Waves and instabilities for model tropical convective parameterizations*, J. Atmos. Sci., 58, b, 896-914, 2001.

[29] A. J. Majda and P. E. Souganidis, *The effect of turbulence on mixing in prototype reaction-diffusion systems*, Comm. Pure Appl. Math., 53, 1284-1304, 2000.

[30] B. E. Mapes and R. A. Houze, *Diabatic divergence profiles in western Pacific mesoscale convective systems*, J. Atmos. Sci., 52, 1807-1828, 1995.

[31] T. Matsuno, *Quasi-geostrophic motions in the equatorial area*, J. Meteor. Soc. Japan, 44, 25-42, 1966.

[32] J. D. Neelin and I. M. Held, *Modeling tropical convergence based on the moist static energy budget*, Mon. Wea. Rev., 115, 3-12, 1987.

[33] J. D. Neelin, I. M. Held and K. H. Cook, *Evaporation-wind feedback and low-frequency variability in the tropical atmosphere*, J. Atmos. Sci., 44, 2341-2348, 1987.

[34] J. D. Neelin and N. Zeng, *A quasi-equilibrium tropical circulation model: Formulation*, J. Atmos. Sci., 57, 1741-1766, 2000.

[35] O. M. Pauluis, A. J. Majda and D. M. W. Frierson, *Propagation, reflection, and transmission of precipitation fronts in the tropical atmosphere*, in prep for J. Atmos. Sci., 2004.

[36] J. Pedlosky, *Geophysical Fluid Dynamics*, Springer-Verlag, New York, second edition, 1987.

[37] S. G. H. Philander, T. Yamagata and R. Pacanowski, *Unstable air-sea interactions in the tropics*, J. Atmos. Sci., 41, 604-613, 1984.

[38] J. M. Slingo and co-authors, *Intraseasonal oscillations in 15 atmospheric general circulation models: results from an AMIP diagnostic subproject*, Climate Dyn., 12, 325-357, 1996.

[39] A. H. Sobel, S. E. Yuter, C. S. Bretherton and G. N. Kiladis, *Large-scale meteorology and deep convection during TRMM KWAJEX*, Mon. Wea. Rev., 132, 422-444, 2004.

[40] M. Wheeler and G. N. Kiladis, *Convectively coupled equatorial waves: Analysis of clouds and temperature in the wavenumber-frequency domain*, J. Atmos. Sci., 56, 374-399, 1999.

[41] F. A. Williams, *Combustion Theory*, Benjamin/Cummings Publishing Company, 1985.

[42] J.-I. Yano and K. A. Emanuel, *An improved model of the equatorial troposphere and its coupling to the stratosphere*, J. Atmos. Sci., 48, 377-389, 1991.

[43] J.-I. Yano, J. C. McWilliams, M. W. Moncrieff and K. A. Emanuel, *Heirarchical tropical cloud systems in an analog shallow-water model*, J. Atmos. Sci., 52, 1723-1742, 1995.